Echo-time dependence of the BOLD response transients

NeuroImage 159 (2017) 355–370

Contents lists available at ScienceDirect

NeuroImage

journal homepage: www.elsevier.com/locate/neuroimage

Echo-time dependence of the BOLD response transients – A window into brain functional physiology

Martin Havlicek [*,1], Dimo Ivanov, Benedikt A. Poser, Kamil Uludag

Dept. of Cognitive Neuroscience, Faculty of Psychology and Neuroscience, Maastricht University, 6200MD, Maastricht, The Netherlands

ARTICLE INFO

Keywords:
Multi-echo
BOLD signal
Nonlinear
Transient
Intercept
Intravascular
Extravascular
Time-course

ABSTRACT

The blood oxygenation level-dependent (BOLD) fMRI response to neuronal activation results from a complex interplay of induced metabolic and vascular changes. Thus, its transients, such as initial overshoot and post-stimulus undershoot, provide a window into the dynamic relationships of the underlying physiological variables. In this study, we propose multi-echo fMRI as a tool to investigate the physiological underpinnings of the BOLD signal, in particular, and brain functional physiology, in general. In the human visual cortex at 3 T, we observed that the BOLD response is nonlinearly dependent on echo-time (TE) and the amount of nonlinearity varies during the entire time-course. Fitting a linear model to this nonlinear relationship resulted in a positive intercept at TE = 0 ms. The time-course of the intercept exhibited fast and slow modulations, distinctly different both from the BOLD response and cerebral blood flow (CBF). In order to shed light on the TE-dependence of the BOLD signal and the intercept time-course, we performed simulations based on a nonlinear two-compartmental BOLD signal model combined with the dynamic balloon model. The modeling suggests that the intercept time-course reflects a weighted sum of deoxyhemoglobin concentration and venous CBV signal changes. We demonstrate that only CBF-venous blood volume (CBV) uncoupling but not CBF-oxygen metabolism ($CMRO_2$) uncoupling can fully account for our experimental observations. In particular, these results strongly argue for a slow evolution of the venous CBV together with stimulus-type-dependent CBF transients (the latter being tightly coupled with $CMRO_2$) to be responsible for the BOLD signal adaptation during stimulation and for the post-stimulus undershoot. Thus, BOLD signal transients are composed of smoothed version of neuronal time-course as reflected in CBF and $CMRO_2$ and secondary vascular processes due to biomechanics of venous blood vessels, and multi-echo fMRI in combination with modeling provides invaluable insights into these physiological processes.

1. Introduction

Neuronal activation causes a series of physiological events, including localized changes in cerebral blood flow (CBF), cerebral blood volume (CBV), cerebral metabolic rate of oxygen ($CMRO_2$) and deoxyhemoglobin content (Buxton et al., 2004). These physiological variables form the basis of the blood oxygenation level-dependent (BOLD) signal as measured in functional MRI (fMRI), due to fact that deoxyhemoglobin is paramagnetic and its changes alter the local magnetic susceptibility of blood (Ogawa et al., 1990). Note that next to the BOLD effect, the fMRI signal may also be spatially and temporally influenced by other physiological and physical parameters ((Uludağ et al., 2009) and references therein). The BOLD response to a stimulus exhibits transients, such as response adaptation (also referred to as overshoot) and post-stimulus undershoot, which are the result of dynamic mismatches between the aforementioned physiological variables (e.g. (Buxton, 2001; Hoge et al., 1999; Krüger et al., 1999; Mandeville et al., 1998)). Therefore, the transients can reflect neuronal effects, but also uncoupled vascular effects due to the biomechanics of blood vessels (Chen and Pike, 2009; Havlicek et al., 2015; Mullinger et al., 2013; Sadaghiani et al., 2009; Uludağ et al., 2004).

In addition to physiological variables, the fMRI signal is also dependent on physical measurement parameters, such as magnetic field strength (B_0) and echo-time (TE). The TE-dependence of signal intensity (S) acquired with gradient-echo echo-planar imaging (GE-EPI) is usually approximated by a simple exponential decay ((Uludag and Blinder, 2017)

* Corresponding author. Department of Cognitive Neuroscience, Maastricht Brain Imaging Centre (MBIC), Faculty of Psychology & Neuroscience, Maastricht University, PO Box 616, 6200MD, Maastricht, The Netherlands.
E-mail address: m.havlicek@maastrichtuniversity.nl (M. Havlicek).
[1] Visiting address: Oxfordlaan 55, 6229 ER, The Netherlands.

http://dx.doi.org/10.1016/j.neuroimage.2017.07.034
Received 10 January 2017; Received in revised form 8 July 2017; Accepted 17 July 2017
Available online 18 July 2017

and references therein):

$$S \approx S_0 \cdot \exp\left(-\mathrm{TE} \cdot R_2^*\right), \quad (1)$$

where S_0 refers to the intrinsic signal at TE = 0 ms and R_2^* is the transverse relaxation rate ($= 1/T_2^*$) of gray matter tissue, which primarily depends on blood deoxygenation. Conventional EPI sequences measure the signal at a single TE, typically chosen to match the average tissue T_2^* to maximize the functional contrast-to-noise ratio (CNR); i.e. sensitivity. However, T_2^* values strongly vary across the brain and between subjects and, additionally, are field strength dependent (see e.g. (Cheng et al., 2015; Donahue et al., 2011; Lu and Van Zijl, 2005; Uludağ et al., 2009; Yacoub et al., 2003)).

Using multi-TE data, the BOLD contrast sensitivity can be optimized with weighting schemes that combine fMRI signal at different TEs (Poser and Norris, 2009; Poser et al., 2006; Posse et al., 1999). Moreover, multi-TE data have also been useful in providing insights into underlying physiological changes induced by neuronal activity. It has been used for quantification of stimulation-induced ΔR_2^* changes (Barth et al., 1999; Donahue et al., 2011; Lu and Van Zijl, 2005; Speck and Hennig, 1998), for data denoising that aims to differentiate between BOLD signal changes and imaging artifacts (Kundu et al., 2012), or to classify voxels containing mainly large vessels or micro-vasculature (Barth et al., 2001). In these approaches, it is commonly assumed that the fractional change in the BOLD signal can be described by a single (apparent) transverse relaxation rate that is linearly dependent on TE:

$$\Delta S/S \approx -\mathrm{TE} \cdot \Delta R_2^* + \Delta S_0/S_0, \quad (2)$$

where the slope, ΔR_2^*, can be directly related to the change in deoxyhemoglobin content. The linear relationship with TE is assumed for both activation-induced fractional signal changes and during resting-state (Kundu et al., 2013, 2015; Peltier, 2002). Importantly, it is typically believed that this linear dependence holds during both steady-state and transient periods of the fMRI response. Any non-zero intercept, $\Delta S_0/S_0$, is usually assigned to non-BOLD sources, such as inflow effects, elevation in extravascular proton density and head motion artifacts (Barth et al., 1999; Gao and Liu, 2012; Jochimsen et al., 2005; Kundu et al., 2012; Speck and Hennig, 1998; Stroman et al., 2002, 2003).

There are only few studies that specifically investigated the TE-dependence of the BOLD response transients. At 9.4 T in a visual cortex of an anesthetized cat, Zhao et al. (2007a) reported linear TE-dependence of both the positive BOLD response and post-stimulus undershoot with significant positive and small negative intercepts, respectively. In human subjects at 4 T, Yacoub et al. (2001) observed that the size of the initial dip increases with TE. Their data acquired at three TEs suggest only roughly linear dependence and a small negative intercept at TE = 0 ms. It should be noted that these studies relied only on few TEs (2–4), which might provide less accurate estimates of the slope and the intercept and may not be able to reveal nonlinear TE dependencies.

To shed light on the TE-dependence of the fMRI signal, it is important to realize that the fMRI signal has both extravascular (EV) and intravascular (IV) components, and their relative contributions are dependent on the field strength, imaging technique and TE (e.g. (Uludağ et al., 2009; Yacoub et al., 2003)). In addition, the CBV of the various vascular compartments also affects the relative amount of EV and IV signals. While the fractional changes in EV signal are well established to be approximately linearly dependent on TE (Donahue et al., 2011; Gati et al., 1997; Ogawa et al., 1993; Yacoub et al., 2003), theoretical simulations predict nonlinear TE-dependence of the IV signal (Boxerman et al., 1995; Duong et al., 2003; Lee et al., 1999; Marques and Bowtell, 2004, 2006, 2008). It was proposed by Jin et al. (2006) that the non-zero intercept obtained from a linear analysis (Eq. (2)) might also originate from a linear fitting to a nonlinear relationship between $\Delta S/S$ and TE. This study showed that this is due to significant contribution of IV signal at shorter TEs, supported by the observation that the nonlinear dependence disappeared after suppressing the IV signal using diffusion weighting. Therefore, the authors suggested that, if the fractional BOLD signal changes diverge from a linear TE-dependence (Eq. (2)), the two-compartment model including EV and IV signals has to be utilized.

In this paper, we demonstrate nonlinear TE-dependence of the BOLD response and its transients observed in the tissue parenchyma of human visual cortex at 3 T during two experimental conditions of static and flickering visual stimuli. We observed that the amount of nonlinearity dynamically changes during stimulation as well as after the end of stimulation. While the nonlinear TE-dependence can be related to the aforementioned non-zero contribution of the IV signal, the dynamic deviation during transient periods indicates time-dependent uncoupling between CBF and other physiological variables, such as CBV or $CMRO_2$. To support this hypothesis and to assess dependence of response transients on experimental manipulation, additional CBF data were acquired and compared with the BOLD data. Furthermore, we propose that the calculated intercept time-course, obtained by linear fitting of the TE-dependent fractional BOLD signal changes, provides additional information about the underlying physiological variables. Thus, the intercept may not only represent imaging artifacts, as previously suggested (e.g. Kundu et al. (2012)), but also physiological parameters, such as CBV and deoxyhemoglobin concentration. To support this hypothesis, we simulate the impact of various physiological scenarios on the TE-dependence of the BOLD signal using a two-compartmental model of the fMRI signal. These simulations allow us to test two competing hypotheses about the physiological origins of the fMRI response transients (in addition to direct CBF contribution), i.e. caused either by a CBF-CBV uncoupling (Buxton et al., 1998; Chen and Pike, 2009; Mandeville et al., 1999; Yacoub et al., 2006) or a CBF-$CMRO_2$ uncoupling (Donahue et al., 2009; Frahm et al., 2008; Hua et al., 2011; Lu et al., 2004; Poser et al., 2011; van Zijl et al., 2012). Our results suggest that a slow evolution of CBV rather than that of $CMRO_2$ is responsible for the early-overshoot and for the post-stimulus undershoot, in addition to the variable CBF contribution (see, e.g. (Sadaghiani et al., 2009)). Thus, the BOLD response transients and their TE-dependence provide a window into the physiological processes underlying the hemodynamic response and brain functional physiology.

2. Materials and methods

2.1. Experimental data

2.1.1. Data acquisition

MR imaging was performed on a 3 T Siemens Prisma Fit scanner (Siemens Medical Solutions, Erlangen, Germany). Five healthy volunteers (three males, age range: 25–34) were scanned using the standard 64-channel head-neck coil. The subjects gave informed consent prior to the scanning, according to the guidelines of the local ethics committee of the Faculty of Psychology & Neuroscience, Maastricht University.

For each subject, a localizer scan was acquired, followed by a total of ten functional runs and one anatomical scan: 6 multi-TE EPI runs, interleaved with 4 arterial spin labeling (ASL) runs and an MPRAGE acquisition. BOLD measurements were performed using a multi-TE gradient-echo EPI sequence (Poser et al., 2006). Thirteen oblique slices with no inter-slice gap were acquired in interleaved fashion, covering early visual areas. The imaging parameters were: TR = 3300 ms with acquisition delay of 2000 ms (i.e. to minimize the inflow effect to the measured BOLD signal (Gao and Liu, 2012)); 217 volumes (total scan duration 12 min); FOV = 192 × 192 mm^2; nominal voxel size = 3 × 3 × 3 mm^3, flip angle = 90°; matrix size = 64 × 64; inter-echo spacing = 0.5 ms, six TEs = 8, 20, 33, 45, 57, and 70 ms. To achieve short readouts and inter-echo spacing, GRAPPA parallel imaging with an acceleration factor 2 (Griswold et al., 2002) and 6/8 partial Fourier were used.

To measure the relative CBF change, perfusion weighted imaging was performed using a single-TE FAIR-Q2TIPS ASL sequence (Kim, 1995)

with a 3D GRASE readout (Vidorreta et al., 2013). Eighteen oblique slices were acquired overlapping with the brain coverage of the BOLD EPI data. The imaging parameters were: nominal voxel size = 3 × 3 × 3 mm^3; TR = 2200 ms; 250 volumes (scan duration 9 min 10 s); TI1 = 700 ms; TI2 = 1800 ms; TE = 22 ms.

Finally, T1-weighted anatomical images of the whole brain were acquired using MPRAGE sequence (Mugler and Brookeman, 1990): 1 mm isotropic nominal voxel size and FOV = 224 × 224 mm^2; matrix size = 224 × 224; TE = 2.1 ms; TR = 2400 ms; TI = 1040 ms; 8° flip angle; GRAPPA 2; no partial Fourier; scan duration 6 min 14 s.

2.1.2. Visual stimulation

An experiment enabling stimulus-dependent neuronal modulation of the BOLD response transients (i.e. adaptation of the positive response and the size of the post-stimulus undershoot) was performed using visual stimulation (see (Havlicek et al., 2015; Sadaghiani et al., 2009) for details). The subjects were instructed to fixate on a small dot at the center of the screen throughout the experiments. Each of the EPI functional runs began with a 55 s resting period and continued with alternation of two static and two flickering checkerboard conditions (each 55 s long), interspersed with 110 s resting periods. Note that the resting period was twice as long as the activation period in order to allow for a full recovery of the post-stimulus BOLD undershoot (Frahm et al., 1996; Krüger et al., 1999; Sadaghiani et al., 2009). The order of static and flickering conditions within a run was pseudo-randomized. For the static condition, a full-field, black-and-white radial checkerboard was presented (Michelson contrast 1), whereas, for the flickering condition, reduced contrast (Michelson contrast 1/3) checkerboards were presented at 4 Hz (8 reversal per second). The resting periods consisted of a gray screen isoluminant with the mean luminance of the checkerboard. In order to maintain the subjects' attention, the color change of the fixation dot (altering between red and blue at three pseudo-random intervals within each stimulation block) was passively observed.

The ASL functional runs used the same stimulation paradigm as described above, but containing only alternation of three stimulation blocks within each run (i.e. static, flickering, static, or flickering, static, flickering). The number of static and flickering conditions was counterbalanced between runs. The main role of the ASL data was to determine the variable CBF (i.e. neuronal (Uludag and Blinder, 2017), and references therein) contributions to the BOLD response transients and differentiate them from other vascular or metabolic sources.

2.1.3. Data analysis

Extraction of the signal time-courses was performed in two steps, separately for each subject. First, standard statistical methods were applied to select a set of early visual cortex voxels that were activated during the static and flickering conditions. Second, BOLD and ASL time-courses were extracted from selected voxels and further analyzed. Note that time-courses for static and flickering conditions were obtained from the same set of voxels, but the set of selected voxels were independently selected for the BOLD and the ASL data.

The data were preprocessed using SPM12 (R6470) (http://www.fil.ion.ucl.ac.uk/spm). To correct for head motion, realignment parameters were estimated using the fourth TE BOLD data (TE_4 = 45 ms to be consistent with the functional analysis, see below) and the same realignment parameters were applied to the corresponding volumes of all the remaining five echo-times. For the ASL data, the realignment was performed separately for the tagged and control images. The mean tagged image was then coregistered to the mean control image and the spatial transformation matrix was applied to all tagged images. Similarly, the mean BOLD and the mean control image were coregistered to the anatomical image and the estimated spatial transformation matrix was applied to the corresponding BOLD and ASL functional data.

For each subject, multi-TE BOLD data were modeled voxel-wise using a general linear model (GLM) in SPM12. This model included predictors representing periods of static and flickering visual stimulation (generated by a convolution of the stimulation boxcar function with a standard double-gamma hemodynamic response function). Data were high-pass filtered (cut-off = 1/400 s) to remove low frequency signal drifts. A first-order autoregressive model was used to remove serial correlations in the data. Finally, a binary mask covering early visual cortex was created from the conjunction of static and flickering image contrasts using the fourth TE only (TE = 45 ms, approximates T_2^* for maximum functional contrast in gray matter at 3 T, see Fig. 2), statistically thresholded at $p < 0.05$ and corrected for family-wise errors (FWE). This binary mask in combination with other criteria was later used to extract BOLD time-courses at each echo-time, as described below.

Similar modeling was performed on the ASL data, with the modification that the design matrix was further augmented with predictors representing perfusion baseline and changes in CBF due to neuronal activation (Havlicek et al., 2017; Hernandez-Garcia et al., 2010; Mumford et al., 2006). As above, using the conjunction of the static and flickering contrasts and a statistical threshold, we obtained binary mask for voxels activated in CBF, which was then used to extract ASL time-courses. The CBF time-course was obtained from the ASL time-course using surround subtraction (Liu et al., 2002; Mumford et al., 2006) and the representative CBF responses for static and flickering conditions were calculated by averaging over the corresponding trials across all 4 runs and all selected voxels. Note that about 160 voxels were extracted for each subject. Using these voxels, average CBF responses for static and flickering stimuli (later averaged also across subjects) were expressed in percent signal change relative to the initial baseline period (i.e. 50 s at the beginning of each run).

2.1.4. Analysis of the TE-dependence of the BOLD response

To indicate the spatial distribution of tissue-specific T_2^* values, T_2^* maps were generated under the assumption of a mono-exponential signal decay model (Eq. (1)), where $T_2^* = 1/R_2^*$. The T_2^* values (together with S_0) were then estimated from the signal intensities, $S(\mathrm{TE})$, at the six TEs using a nonlinear least squares algorithm (Levenberg-Marquardt algorithm, Matlab function *lsqnonlin*). Note that the voxel-specific signal intensity, $S(\mathrm{TE})$, represents a signal baseline (for each TE) during rest, obtained by averaging over the first 50 s from all six BOLD functional runs of a given subject. The smoothed distribution of T_2^* values (obtained using Matlab function *ksdensity*), representing the masked voxels within the visual cortex, were estimated for each subject separately. The main peak of T_2^* value distribution was identified for each subject, and voxels with T_2^* values ±5 ms around the peak were selected for further analysis. With this procedure, we reduced the partial voluming with cerebrospinal fluid (CSF) and white matter voxels having higher or lower T_2^* compared to the gray matter tissue voxels, respectively. Based on this procedure, 120–170 voxels were included from the original subject-specific binary mask. Note that these voxels highly overlapped with voxels selected based on the CBF activation mask (see Fig. 2 and Table S1).

Using these voxels, average BOLD responses for static and flickering stimuli were expressed in percent signal change relative to the pre-stimulus baseline and plotted for the different echo-times. The baseline values were determined using the first 50 s at the beginning of each run. Additionally, to explore the TE-dependence of the BOLD response transients, the average BOLD responses were also normalized with respect to the end of stimulation. Next, the TE-dependence of BOLD percent signal change was analyzed assuming linear dependence with Eq. (2), where the slope, ΔR_2^*, and the intercept, $\Delta S_0/S_0$, were fitted to the six TEs of the averaged BOLD responses. This analysis was first performed on the TE-dependent signal averaged over three temporal windows assigned to: 'early-overshoot' of the positive response (10–20 s); 'steady-state' by the end of stimulation (45–55 s); and the post-stimulus undershoot (70–80 s). Later, the same analysis was repeated but individually for each time point of the TE-dependent BOLD responses. The divergence of the TE-dependence from a linear relationship was further studied by

normalizing the TE-dependent BOLD signal changes with respect to the longest TE (i.e. 70 ms) in the three temporal windows mentioned above.

2.2. Simulations

To test different hypotheses regarding the source of TE-dependency of the BOLD signal changes, we performed simulations by assuming a two-compartment model of the BOLD fMRI signal. The baseline BOLD signal, $S(\mathrm{TE})$, is modeled as blood volume-weighted sum of EV and IV signals, S_{EV} and S_{IV}:

$$S = (1 - V_0)\cdot S_{EV} + V_0\cdot S_{IV}. \quad (3)$$

In this model, we assume that the BOLD signal at 3 T acquired using a GE sequence originates primarily from post-capillary venous vessels and neglect the small contribution from arterioles and capillaries (Uludağ et al., 2009). Therefore, V_0 represents the baseline venous blood volume fraction. Further, the contribution of EV and IV signals can change with TE; i.e. for 3 T at short TE, the BOLD signal is dominated by the IV component, while at longer TEs it is largely dominated by the EV component.[2] In general, TE-dependence of the EV signal can be well described using single-exponential, whereas the TE-dependence of the IV signal can be more accurately characterized using e.g. the Luz-Meiboom exchange model (Duong et al., 2003; Luz and Meiboom, 1963). Detailed description of this model is beyond the scope of this paper. However, for illustration purposes, we show the exemplary TE-dependence of the baseline IV and EV signals in Fig. 1A and their intrinsic baseline ratio, $\varepsilon = S_{IV}/S_{EV}$, in Fig. 1B. In our modeling, we considered directly the ratio, ε, which subsumes different (nonlinear) TE-dependencies of the baseline IV and EV components.

During neuronal activation, the transverse relaxation rates of the EV, R^*_{2E}, and IV, R^*_{2I}, signals are altered by incremental amounts ΔR^*_{2E} and ΔR^*_{2I}, respectively, and the venous blood volume changes to a new value V. Thus, the fractional change of BOLD signal is equal to (Obata et al., 2004):

$$\frac{\Delta S}{S} = \frac{(1-V)\cdot\exp\left(-TE\cdot\Delta R^*_{2E}\right) + \varepsilon\cdot V\cdot\exp\left(-TE\cdot\Delta R^*_{2I}\right) - (1-V_0) - \varepsilon V_0}{1 - V_0 + \varepsilon\cdot V_0}. \quad (4)$$

This is an exact expression for the BOLD signal change, given the assumptions described above. Then, by considering diffusion and chemical exchange mechanisms that relate the changes in transverse relaxation rates of EV and IV signals to changes in blood oxygenation (Ogawa et al., 1990) and by following the derivation of the BOLD signal equation by Stephan et al. (2007), which fully preserves the contribution of the IV signal change, the fractional change of BOLD signal is approximately:

$$\frac{\Delta S}{S} \cong V_0\left[c_1\cdot(1-q)\cdot\mathrm{TE} + c_2\cdot\left(1 - \frac{q}{v}\right)\cdot\varepsilon\cdot\mathrm{TE} + (1-v)\cdot(1-\varepsilon)\right]. \quad (5)$$

This expression includes the key physiological variables underlying the BOLD signal, i.e. changes in the deoxyhemoglobin content, $q = Q/Q_0$, and in the venous CBV, $v = V/V_0$, both normalized with respect to their baseline values. Here, the first term in the square brackets represents the change in EV signal. It is fully determined by the change in deoxyhemoglobin content that is linearly dependent on TE. The second term expresses the change in IV signal including the change in venous CBV, which is determined by the deoxyhemoglobin to blood volume ratio; i.e. the deoxyhemoglobin concentration. Hereafter, we always refer to the second term simply as the change in IV signal. In contrast to the change in EV signal, the IV component is nonlinearly dependent on TE via ε. With activation, the IV signal results in a positive change. As shown in Fig. 1C, for 3 T, GE sequence and mostly tissue parenchymal voxel content, the contribution of IV signal change with activation is expected to peak between TE≅ 20–50 ms but diminishes with longer TEs (Duong et al., 2003; Marques and Bowtell, 2006, 2008; Zhao et al., 2007b). In Eq. (5) this characteristic nonlinear TE-dependence of IV signal change is given by $\varepsilon\cdot$TE. Both EV and IV components are further scaled by (positive) TE-independent constants c_1 and c_2 (see Supplementary material for details). Finally, the third term represents the change in the effective proton spin density due to volume changes of the EV and IV compartments. It is determined by the change in venous CBV and is also nonlinearly dependent on TE via the variable ε. As mentioned above, we assume that for 3 T and GE sequence $\varepsilon > 1$ at very short TE and $\varepsilon < 1$ at longer TE (see Fig. 1B), in accordance with theoretical simulations (Duong et al., 2003; Uludağ et al., 2009). Thus, with activation and short TE ($\varepsilon > 1$), the third term $(1-\varepsilon)\cdot(1-v)$ results in a positive blood volume contribution to the BOLD signal, whereas for longer TE ($\varepsilon < 1$), the third term has negative contribution to the BOLD signal.

In order to model the TE-dependence of the BOLD response also during transient periods, the BOLD signal equation (Eq. (5)) was combined with the balloon model (Buxton et al., 1998, 2004) that describes the effects of hemodynamic changes on the BOLD signal. The balloon model represents a mass balance for blood volume and deoxyhemoglobin as they pass through the venous compartment. The dynamic changes in v and q are driven by changes in CBF and $\mathrm{CMRO_2}$ that are associated with brain activation (see Supplementary Material for details). Based on this model, we hypothesized that the TE-dependence of the BOLD response transients can be explained by two scenarios in which there is dynamic transient uncoupling between two hemodynamic parameters: (I) CBF and venous CBV or (II) CBF and $\mathrm{CMRO_2}$.

- In Scenario I, we assumed that, during steady-state, CBF and CBV are coupled via a power law relationship (Grubb et al., 1974), with exponent $\alpha = 0.3$, whereas during the transient periods venous CBV changes more slowly than CBF; i.e. reaching the steady-state by the end of the stimulation and recovers more slowly to baseline than CBF after stimulus cessation. Additionally, we assume a constant[3] $\Delta\mathrm{CBF}/\Delta\mathrm{CMRO_2}$ coupling parameter $n = 3$.
- In Scenario II, the CBF and venous CBV were assumed to be coupled during both transient and steady-state periods with $\alpha = 0.3$. Importantly, the $\mathrm{CMRO_2}$ variable was considered uncoupled from CBF, with a dynamic delay comparable to CBV in the Scenario I and $n = 3.5$ during the steady-state at the end of stimulation (as n is defined only during steady-states).

The size of the uncoupling (i.e. mismatch of venous CBV or $\mathrm{CMRO_2}$ with CBF) was chosen to accommodate the length of the post-stimulus undershoot in the experimental BOLD responses for the static stimulus, as for this case the CBF contribution to the BOLD signal undershoot is small (see below for details). In both scenarios, the CBF responses were modeled to closely resemble the experimental CBF responses; i.e. exhibiting the same percent signal changes and response transients. In this sense, the CBF responses and their transients, reflecting stimulus-dependent neuronal modulation, pre-determined the variable CBF contribution to the BOLD response transients, and thus allowed independent assessment of the aforementioned scenarios. The IV-to-EV ratios for six echo-times $\mathrm{TE}_{1-6} = [8,\ 21,\ 33,\ 45,\ 58,\ 70]$ ms were chosen as

[2] Modeling of EV and IV can be very complex, as it depends on vascular (arterial, capillary and venous) and tissue composition of the imaged voxel, chemical/diffusion exchange, vessel orientation with respect to the magnetic field, etc. Nevertheless, the main effects at 3 T for GE are accurately represented with the following simulations.

[3] Note that with the constant coupling n in Scenario I, we assume a tight linear relationship between CBF and $\mathrm{CMRO_2}$. This is clearly a simplification of our simulation as, in general, the relationship can be nonlinear as described e.g. by the limited oxygen extraction model (Buxton and Frank, 1997; Havlicek et al., 2015). Nevertheless, this simplification has no effect on the model comparisons and conclusions presented in this paper.

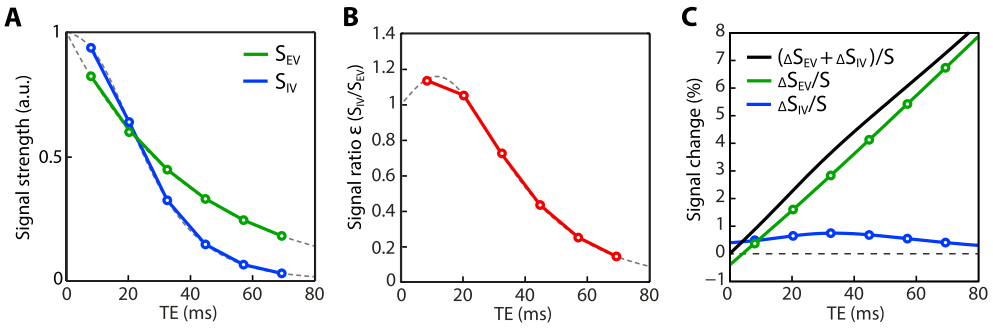

Fig. 1. Illustration of the TE-dependence of the IV and EV signal at rest (A), their intrinsic ratio (B), and expected percent signal changes due to activation (C), where the solid black line represents the total signal change in BOLD signal. Negative intercept of EV signal at TE = 0 ms indicates the effect of CBV-induced reduction of water molecules, as in the VASO effect (Huber et al., 2014b; Lu et al., 2003). The TE-dependencies were generated using a mono-exponential decay model for EV signal and the Luz-Meiboom model for IV signal, by assuming parameterization for 3 T and GE sequence (Duong et al., 2003; Griffeth and Buxton, 2011; Lu and Van Zijl, 2005; Uludağ et al., 2009), resting venous blood volume fraction and blood oxygenation: $V_0 = 0.03$ and $Y_0 = 0.6$, and their new values due to activation: $V = 0.036$, and $Y = 0.65$.

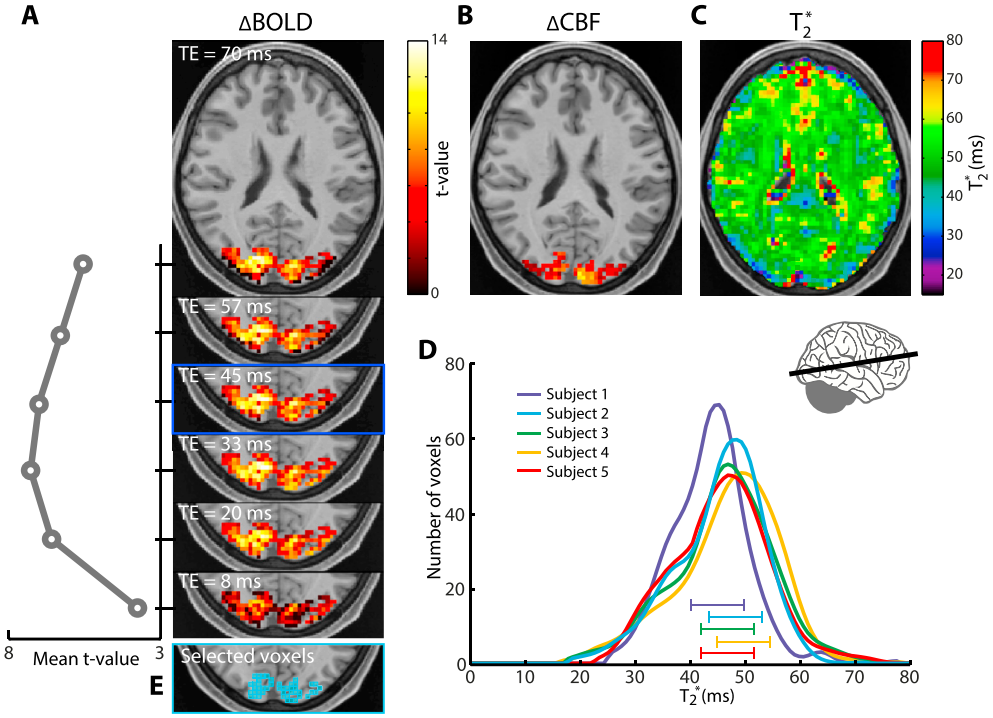

Fig. 2. Maps of the t-statistics for BOLD at the various TEs from an individual subject, overlaid on a single-slice of the anatomical data (A). The activation maps represent the conjunction between static and flickering conditions. They were masked with the thresholded map of the fourth TE ($p < 0.05$, FWE) – highlighted with a blue frame. The plot on the left side represents the TE-dependence of the mean *t*-value (averaged across voxels included in the activation mask). The CBF-related activation map of the conjunction between static and flickering stimuli ($p < 0.05$, FWE) are presented in (B) and a map of the estimated T_2^* values at rest in (C). Subject-specific distributions of estimated T_2^* are shown in (D), marking the ±5 ms range around the individual peaks and the resulting voxel mask (i.e. an individual subject's example of a single-slice) is displayed in (E).

$\varepsilon(\mathrm{TE}) = [1.15,\ 1.05,\ 0.75,\ 0.45, 0.25,\ 0.15]$ (see Fig. 1B). The resting venous blood volume fraction was fixed to $V_0 = 0.03$. All the parameters values mentioned above, represent commonly assumed values in theoretical simulations, which we fine-tuned based on an initial grid-search procedure within physiologically plausible ranges (Buxton et al., 2004; Griffeth et al., 2013; Obata et al., 2004). These scenarios (including combinations of both $CMRO_2$ and CBV uncoupled from CBF, see Supplementary Material for further details) were tested for both the static and flickering conditions.

For both scenarios, the TE-dependencies of the BOLD response transients were compared to the experimental data. In addition, the slope and intercept time-courses resulting from the linear regression analysis of the simulated TE-dependent BOLD data were determined.

3. Results

3.1. Experimental data

Fig. 2A shows maps of BOLD *t*-statistics from a representative subject (for a conjunction of static and flickering conditions), illustrating the TE-dependence of the BOLD contrast within the visual cortex. The activation map at $TE_1 = 8$ ms has on average the lowest t-values. The t-values increase up to $TE_3 = 33$ ms, where we see larger amount of activated voxels with higher t-values. Then for $TE_{4\text{-}6} \geq 45$ ms, t-values tend to slightly decrease – especially in the voxels located closer to the CSF boundary. Note that the activation maps shown are masked with respect to the statistical threshold of the fourth TE map, but there was almost no

difference between voxel mask generated using statistical map utilizing the third or the fourth TE. Next, Fig. 2B shows the activation map obtained from the CBF data. The spatial extent of the CBF activation is more localized compared to the activation in the BOLD data (e.g. at $TE_4 = 45$ ms). The majority of significantly active voxels in the CBF map overlapped with the mask based on BOLD data (see Table S1).

Fig. 2C shows the map of calculated T_2^* values in the same subject. Within the visual cortex defined by the BOLD activation mask at TE = 45 ms, T_2^* values range mostly between 25 and 65 ms, as shown in the plot depicting T_2^* distributions for all individual subjects (see Fig. 2D). There, we see that the main peak is at 47.0±0.8 ms, which is in a good agreement with reported T_2^* values corresponding to tissue parenchyma of the visual cortex at 3 T (e.g. (Lu and Van Zijl, 2005)). Additionally, a smaller bump is present at 34.2±1.0 ms, which most likely represent contribution from smaller vascular components (larger vein compartments are known to have even shorter $T_2^* \sim 22$ ms at 3 T (Triantafyllou et al., 2011)), but it can be also due to partial voluming with white matter or CSF. In the same plot, we show five subject-specific windows of 10 ms around the main peaks that define ranges of T_2^* values corresponding to the final set of selected voxels, in which we expect mainly tissue-weighted voxels (see Fig. 2E for a single slice example). Subject-specific number of selected voxels and their percent overlap with CBF activation map is listed in Table S1.

Fig. 3A shows the average BOLD responses (in percent signal change) to static and flickering stimuli plotted for the six echo-times. All responses show an increase with stimulus onset, reaching their peaks at ~13 s after the stimulus onset, followed by a response adaptation towards the end of stimulation. The response adaptation is stronger for the static stimuli. After stimulus cessation, all responses dip below baseline, reaching the negative peak of post-stimulus undershoot at ~14 s after stimulus cessation. From this point, it takes ~80 s to fully recover to baseline. Note that the post-stimulus undershoot for flickering stimulus is stronger (about twice the amplitude) than for the static stimulus, which makes the signal change during post-stimulus undershoot almost as strong as the signal change during the positive response. These observations were consistent across all six TEs and all five subjects (see error bars in Fig. 3A).

In general, one can see that the signal change of the BOLD response increases with TE. Thus, the positive peak of BOLD responses to static stimuli ranges between ~0.8% (for the shortest TE) and ~6.8% signal change (for the longest TE). The range of signal change is similar but slightly higher for the flickering stimulus. While the range of the negative peak of post-stimulus undershoots after static stimuli is between ~0.2% (for the shortest TE) and ~3.2% (for the longest TE), after the flickering stimulus this range is between ~0.7% and ~6.7% of the signal change.

After normalization of the average BOLD responses with respect to the end of the stimulation block, additional TE-dependent changes of the BOLD response were observed. In Fig. 3B, it can be seen that there is a pronounced dependence of the BOLD response transients (overshoot and post-stimulus undershoot) on TE. In other words, for the shortest TE, the least response adaptation and the smallest post-stimulus undershoot were observed, whereas for the longest TE the largest response adaptation and post-stimulus undershoot. That is, the response amplitudes at different time points do not follow the same TE-dependence (see below). The size of this effect is larger for the positive responses to static stimuli.

Fig. 4A displays the TE-dependence of the BOLD signal for the five subjects, averaged over the three time-windows representing the early-overshoot, steady-state and post-stimulus undershoot. For both conditions (Fig. 4A top: static; bottom: flickering), during early-overshoot and steady-state, the TE-dependence shows a stronger divergence from a

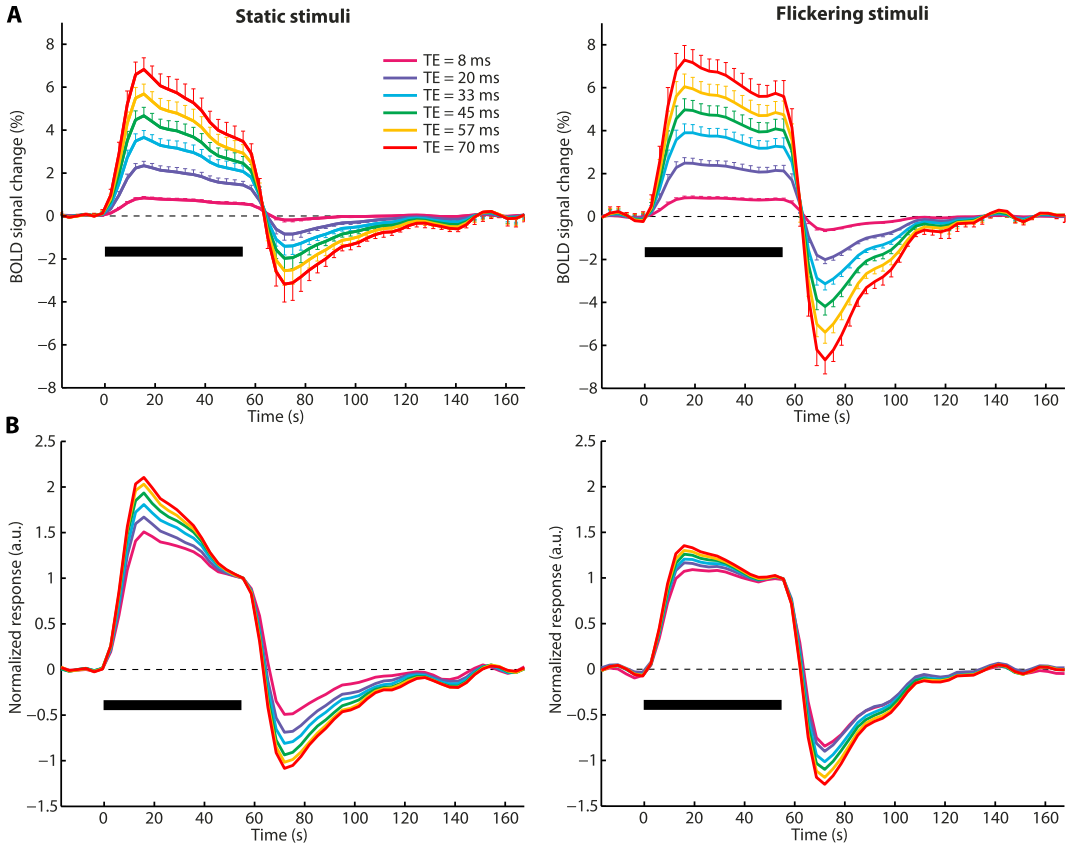

Fig. 3. Top row (A) shows the averaged BOLD responses (n = 5) to static (left) and flickering (right) stimuli plotted for the six different TEs (in percent signal change). A black bar under the time-courses indicates the 55 s period of visual stimulation and the error-bars stand for standard error of the mean. Notice the small oscillations during the later phase of the post-stimulus BOLD undershoot recovery to baseline. However, a detailed investigation of this phenomenon is beyond the scope of this paper. Bottom row (B) shows the same BOLD responses, but normalized with respect to the end of stimulation.

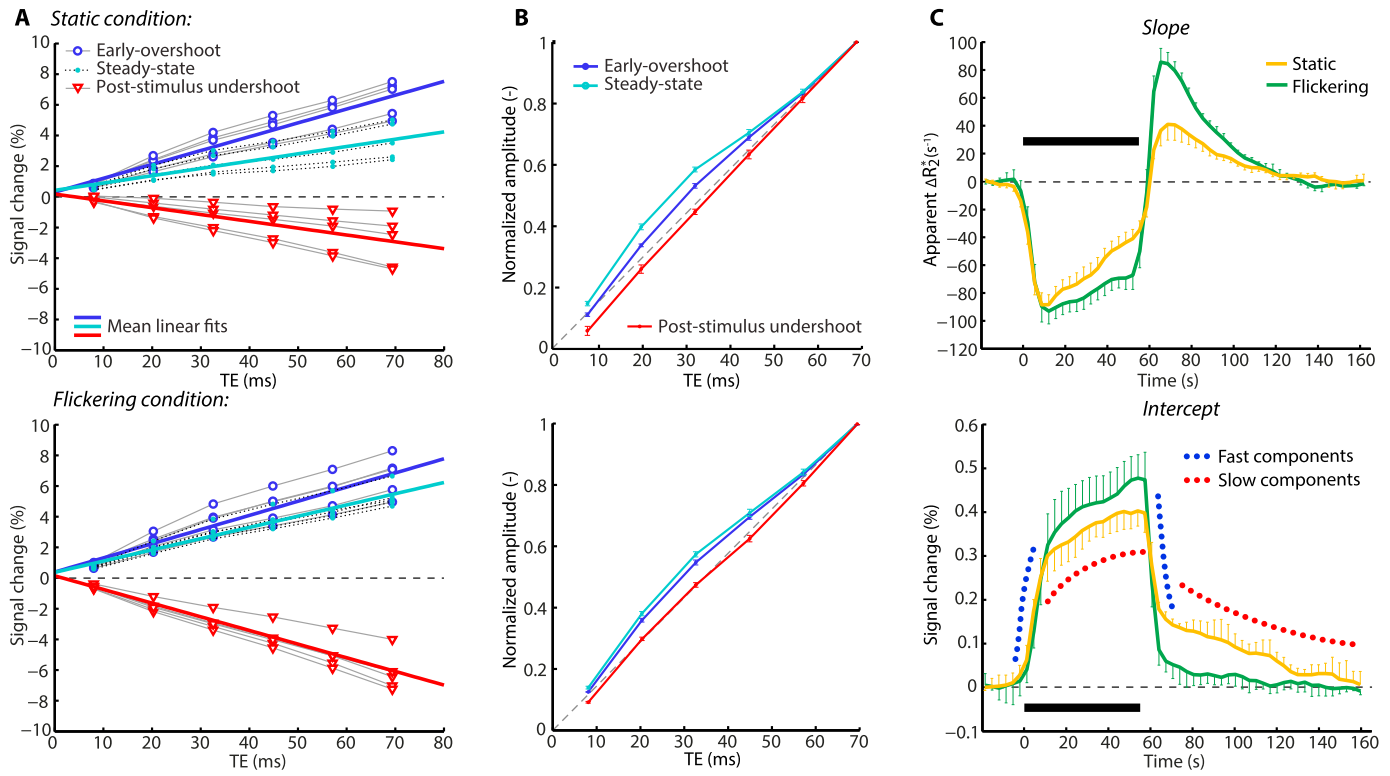

Fig. 4. The percent signal change vs. TE for both static (top) and flickering (bottom) conditions obtained by averaging over the three time-windows of the BOLD responses (early-overshoot, steady-state and post-stimulus undershoot) is shown for the five individual subjects (purple circles, cyan dots and red triangles, respectively) (A). Additionally, the mean linear fits to TE-dependence of the early-overshoot (purple line), steady-state (cyan line) and post-stimulus undershoot (red line) are also shown. Normalized TE-dependent BOLD signal changes with respect to the longest TE (i.e. 70 ms) for the three time-windows, averaged across all subjects, including error-bars representing the standard error of the mean (B). The average time-courses of the calculated slope (i.e. apparent ΔR_2^*) and intercept for both static (orange line) and flickering (green line) stimuli (C, top and bottom, respectively). Red and blue dotted curves around the intercept time-course illustrate the fast and slow response components, respectively. The error-bars represent the standard error of the mean based on five subjects.

linear relationship, whereas a more linear relationship is seen during the post-stimulus undershoot. By fitting a linear model (Eq. (2)) to all subjects' data in the respective time-windows, we estimated the average slopes (i.e. apparent ΔR_2^*) and intercepts for both conditions (see Table 1). For both conditions, all intercepts were positive, while the slopes were negative for the stimulation and positive for the post-stimulation periods. The intercepts of the steady-state (~0.4%) were always larger than those of the early-overshoot, but this difference was statistically significant only for the static condition (two-tailed t-test: $p = 0.0052$ for static and $p = 0.071$ for flickering). Although the intercepts of the early-overshoot and steady-state during the flickering stimulus were slightly larger than during the static stimulus, these differences were not significant (two-tailed paired t-test: $p = 0.2553$ for early-overshoot and $p = 0.1545$ for steady-state). The intercepts of the post-stimulus undershoots after the static and flickering stimuli were smaller compared to the intercepts during the stimulation periods, but still significantly different from zero (two-tailed t-test: $p = 0.0029$ for static and $p = 0.0429$ for flickering). Further, the intercept of the post-stimulus undershoot after the static stimulus was more than twice larger (~0.13%) compared to corresponding intercept (~0.06%) after the flickering stimulus (two-tailed paired t-test, $p = 0.0078$).

Table 1
The estimated slopes (i.e. apparent ΔR_2^*) and intercepts.

	Apparent ΔR_2^* (s^{-1})	Intercept (%)
Static condition:		
Early overshoot	−89.23±7.16	+0.32±0.04
Steady-state	−44.65±7.32	+0.40±0.03
Post-stimulus undershoot	+39.16±8.75	+0.13±0.02
Flickering condition:		
Early overshoot	−93.40±8.63	+0.36±0.06
Steady-state	−70.21±4.96	+0.47±0.06
Post-stimulus undershoot	+86.11±7.83	+0.06±0.02

All values are significantly different from zero at the 0.05 probability level.

The divergence of the TE-dependence from a linear relationship was further studied by normalizing the TE-dependent BOLD signal change with respect to the longest TE (i.e. 70 ms). This normalization removed the main slope differences between conditions and time-windows (including the sign) associated with the apparent ΔR_2^* (as seen in Fig. 4A), and thus allowed for more detailed examination of possibly nonlinear TE dependence. Fig. 4B shows the average normalized profiles of the TE-dependence for the same time-windows and conditions as in Fig. 4A. During both the early-overshoot and steady-state responses to static and flickering stimuli, the normalized BOLD amplitude profiles show a sublinear TE-dependence, with clear elevation between 25 and 45 ms. While the size of this elevation is different between the early-overshoot and steady-state (showing a more pronounced nonlinearity) of the static response, it is more comparable within the flickering response. On the other hand, during the post-stimulus undershoot, the TE-dependence of BOLD amplitudes follows a more linear relationship, especially after the static stimulus. After the flickering stimulus, even though also a more linear TE-dependence is observed, there is some contribution (but much smaller) of a nonlinear component, as in the case of the early-overshoot and steady-state.

In Fig. 4C, we display how the subject-averaged amplitude of the slope and intercept vary over time and how it differs between static and flickering conditions. The slope and intercept time-courses have very distinct behavior over time, suggesting different combination of physiological variables are reflected in these responses. As expected, the responses representing the slope (i.e. the apparent ΔR_2^*) resemble inverted BOLD responses. Since ΔR_2^* is directly related to susceptibility changes caused by a variation in the paramagnetic deoxyhemoglobin content, the shape of the slope is therefore approximately proportional to the change

in deoxyhemoglobin content (see Discussion). In contrast, the intercept has a very distinct time-course. During the entire stimulation interval, it continues to increase for both static and flickering stimuli, with slightly lower amplitude for the static stimulus. In the early phase of stimulation, the responses exhibit a rapid increase that is followed by slow increase. With stimulus cessation, both responses start decreasing but remain positive: For the static stimulus, the amplitude first drops quickly by ~55% and then follows a very slow recovery to baseline, i.e. the full recovery takes >100 s. For the flickering stimulus, the amplitude drops by ~80%, also followed by a slow recovery.

Fig. 5A shows the average time-courses of the CBF responses to static and flickering stimuli that we compared to the BOLD responses acquired at TE = 45 ms, displayed in Fig. 5B. First, the CBF response to the static stimulus exhibits a maximum signal change of ~80%, which is comparable to the maximum CBF response to flickering stimulus (~85%). There is smaller response adaptation in CBF during the flickering stimulus than during the static stimulus, but for both conditions adaptations occur less compared to those of the BOLD responses. Second, the post-stimulus deactivation in the CBF responses is much smaller (with respect to the positive response) compared to the post-stimulus BOLD undershoots. Additionally, the post-stimulus CBF undershoot after the static stimulus is almost negligible. Importantly, neither CBF nor BOLD responses show a dynamic behavior comparable with the intercept (see Fig. 4B).

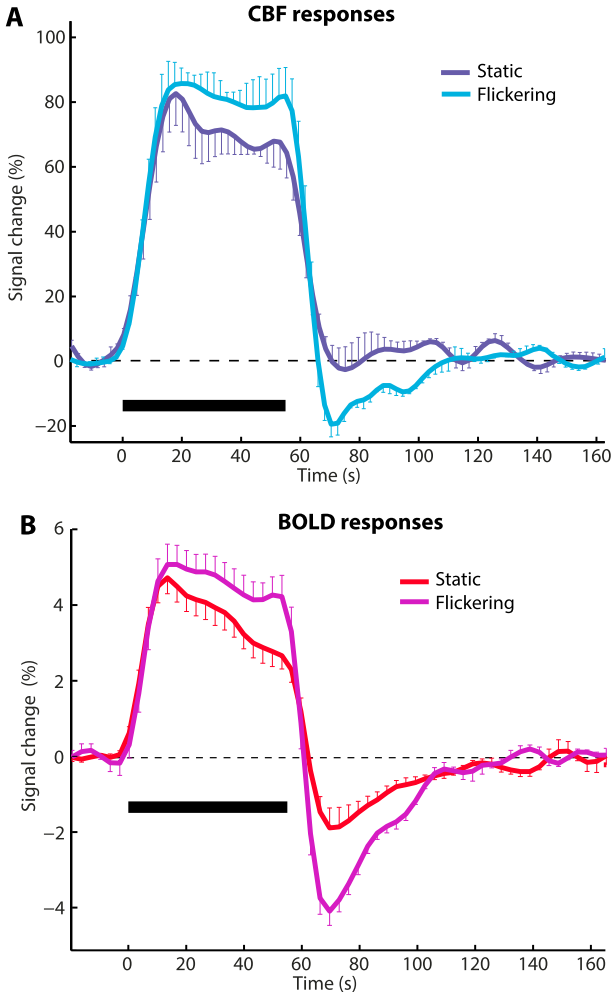

Fig. 5. The average CBF response to static (purple line) and flickering (cyan line) stimuli (A), displayed in percent signal change. The average BOLD response acquired with a TE = 45 ms for both static (magenta line) and flickering (red line) stimuli (B), displayed in percent signal change. The error-bars represent the standard error of the mean based on five subjects. Note that CBF and BOLD responses were acquired during different functional runs, using different MR sequences and temporal resolutions (ASL (TR = 2.2s) and multi-TE (TR = 3.3 s), respectively).

3.2. Simulations

In this section, results are described comparing two tested scenarios of the physiological origins of BOLD response transients such as overshoot and post-stimulus undershoot. For the sake of clarity, below, we fully describe the simulation results only for the static condition and provide complementary results for the flickering condition in the Supplementary Material.

3.2.1. Scenario I: CBF-CBV uncoupling

Fig. 6A–C shows the physiological responses generated under the assumption of CBF-CBV uncoupling. The CBF response is assumed to be similar in shape and amplitude as the experimentally observed (Fig. 6A). The $CMRO_2$ response (cyan) is just a scaled version of the CBF response, with maximum ~27% signal change, and also negligible post-stimulus undershoot. The venous CBV response (blue) has a much slower evolution compared to the CBF response, reaching its maximum (~16%) by the end of stimulation. After stimulus cessation, CBV returns slowly to the baseline. The deoxyhemoglobin response (green), which is determined by the interplay between CBF, CBV and $CMRO_2$, shows a negative change during stimulation, with initial undershoot of ~23%, followed by a pronounced adaptation to ~12% by the end of stimulation, which is followed by a strong post-stimulus overshoot (~9%).

In Fig. 6B, the TE-dependent BOLD responses are shown as generated using Eq. (5). Overall, the BOLD response amplitude increases with TE. After normalization to the amplitude at the end of stimulation for each TE, the BOLD responses reveal a time-varying and nonlinear dependence of the response transient on TE (Fig. 6C); i.e. response overshoot and post-stimulus undershoot are less pronounced at shorter than longer TEs (for flickering condition see Fig. S1). In general, the TE-dependence of the BOLD responses before and after normalization are very comparable to the experimental data (see Fig. 3B). Additionally, a detailed illustration describing the relative contributions of EV, IV and venous CBV signal changes to the BOLD response and how they contribute to possibly nonlinear TE-dependence, as observed during three different temporal windows (in Fig. 4A and B), are presented in the Supplementary Material for both static and flickering conditions (Figs. S3 and S4).

3.2.2. Scenario II: CBF-$CMRO_2$ uncoupling

Fig. 6D–F displays simulation results for the case, where the $CMRO_2$ response is dynamically uncoupled from the CBF response. The venous CBV is tightly coupled with the CBF response, delayed only by ~1 s. In contrast, the $CMRO_2$ response is much slower than the CBF response, having almost the same shape and maximum amplitude (~18%) as the venous CBV in Scenario I. The resulting shape of deoxyhemoglobin response is similar to Scenario I, only exhibiting slightly higher maximum signal change at the initial undershoot (~27%) and post-stimulus overshoot (~11%).

The TE-dependent BOLD responses (Fig. 6E) generated with this scenario of CBF-$CMRO_2$ uncoupling are comparable to the simulated BOLD responses in Scenario I and to the experimental data; i.e. response amplitude increases with TE. Note that at this level both scenarios seem to explain the size of observed BOLD response transients. However, after response normalization, the effect size of the response transient dependence on TE given by Scenario II is very small (especially for the overshoot), which does not compare well with the experimental data. By saying that, one can optimize the contribution of $CMRO_2$ and CBV responses to the BOLD signal (by varying α and n within their physiological limits) and scale the baseline IV-to-EV signal ratio, ε, to obtain comparable TE-dependence of BOLD response transients after response normalization (data not shown). Nonetheless, BOLD response amplitudes (in percent signal change) then follow a different TE-dependency compared to the experimental data (see Discussion for details).

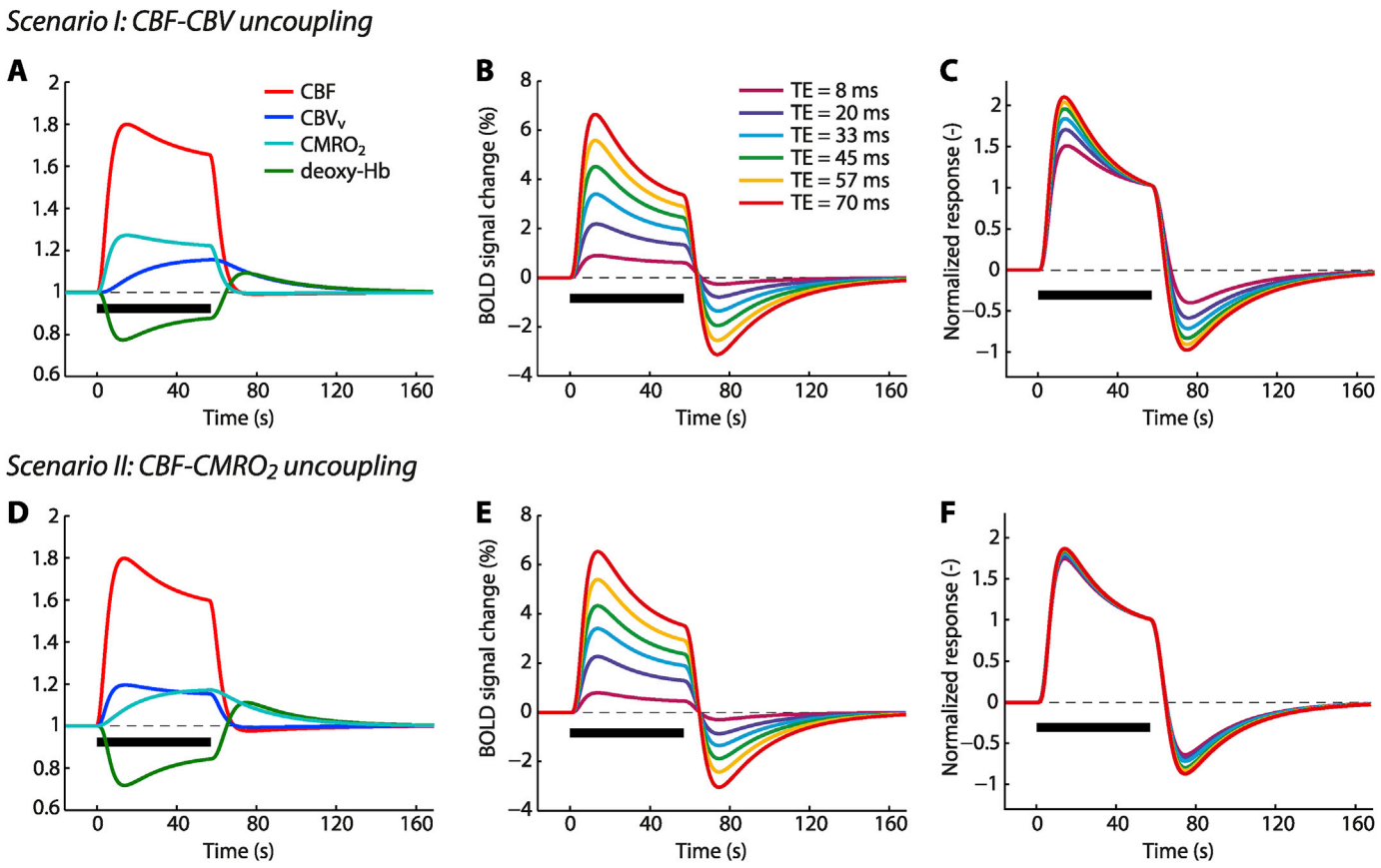

Fig. 6. Results of the theoretical simulations obtained with Scenario I simulating CBF-CBV uncoupling (A-C); Scenario II simulating CBF-CMRO$_2$ uncoupling (D-F). These simulations closely represent the observed signal changes in CBF and BOLD responses to static stimulus. The left plot in each scenario displays time-course of CBF (red line), venous CBV (blue line), CMRO$_2$ (cyan line) and deoxyhemoglobin content (green line). The middle plot shows the BOLD responses for six different TEs (in percent signal change) and the right plot depicts the same BOLD responses after normalization with respect to the end of stimulation. The black bar below the time-courses indicates 55 s period of visual stimulation.

3.2.3. *Intercept indicates a physiological mechanism*

By fitting the linear model (Eq. (2)) to the simulated TE-dependent BOLD responses (Fig. 6B and E), we obtained the slope and intercept time-courses for both tested scenarios. BOLD data generated with a CBF-CBV uncoupling provided a slope and intercept time-courses that are strikingly similar to the slope and intercept time-courses estimated from the experimental data, including the amount of variable percent signal change with time and their relative differences between the static and flickering conditions. In Fig. 7A, we only show the intercept time-courses for both static and flickering conditions. Additionally, in Fig. 7C, we demonstrate the signal composition of the intercept time-course that can be related to components of the BOLD signal equation (but see also Figs. S3 and S4 for more details). The intercept represents a weighted sum of the second and third terms in Eq. (5) that are both nonlinearly dependent on TE component,[4] i.e. the change in IV signal and venous CBV, with weightings reflecting their contributions mainly at shorter TEs. One can notice that during the initial phase of the stimulation, the intercept time-course is dominated mainly by the IV response, whereas, during the later phase of the stimulation, the venous CBV response dominates. During the post-stimulus period following the static stimulus, the intercept is represented almost exclusively by the time-course of venous CBV. However, during the post-stimulus period following the flickering stimulus, both undershoot in IV signal change and elevated venous CBV contributed to the intercept time-course (see Figs. S3 and S4). Note that the slope (i.e. the apparent ΔR_2^*) reflects only the linearly TE-dependent (and most dominant) term in Eq. (5), which is proportional to the change in deoxyhemoglobin content.

From the BOLD data generated with CBF-CMRO$_2$ uncoupling (Scenario II), we estimated the slope that was similar to the experimental data, but the intercept time-course differed dramatically (see Fig. 7B). In particular, the transients in estimated intercept responses do not exhibit continuous increase during stimulation and slow return to the baseline after stimulus cessation. Instead, the intercept response transients resemble the BOLD response itself (see e.g. Fig. 5B).

Finally, simulations exploring the mixed contribution of CBF-CBV and CBF-CMRO$_2$ uncouplings to the post-stimulus BOLD undershoot (in addition to the CBF contribution) are presented in the Supplementary Material (see Fig. S2). These simulations revealed that already a very small relative contribution of the CBF-CMRO$_2$ uncoupling to the post-stimulus undershoot results in intercept time-courses that are not comparable to the ones estimated from the experimental data.

4. Discussion

In this study, we utilized multi-TE fMRI data to study physiological origins of the BOLD response transients. Experimental data and simulations demonstrate that the fMRI response transients reveal information on physiological processes underlying brain functional physiology. Below, we first review the nonlinear TE-dependence of the BOLD response transients observed in the tissue parenchyma of human visual cortex at 3 T. Then, we discuss the intercept time-course at TE = 0 ms estimated with linear regression analysis applied to the TE-dependent BOLD data, and later, we identify causes of the TE-dependence of the response transients and provide interpretation and discuss limitations of

[4] Note that the weights in Fig. 7C were calculated using a linear regression, with $(1-q/v)$ and $(1-v)$ being the explanatory variables generated with Scenario I and then fitted to the intercept response.

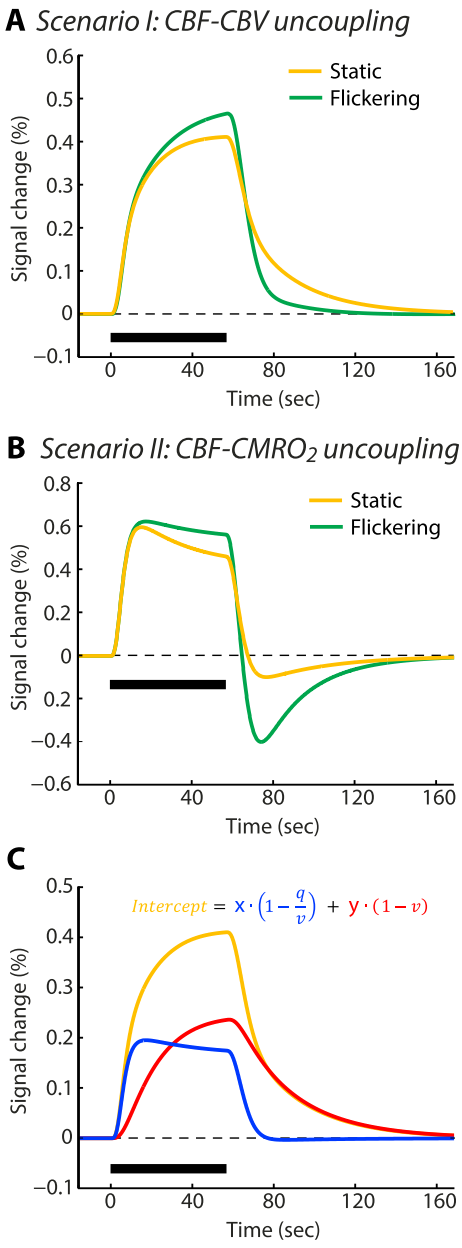

Fig. 7. The calculated intercept time-courses based on the two simulated scenarios: CBF-CBV uncoupling (A) and CBF-$CMRO_2$ uncoupling (B), displayed for both static (orange line) and flickering conditions (green line). The intercept time-course obtained from a CBF-CBV uncoupling for the static condition (C) is given by a sum of changes in the IV (blue line), $(1 - q/v)$, and venous CBV (red line), $(1 - v)$, signals weighted by coefficients $x = 0.75$ and $y = -1.5$, respectively.

the intercept using simulations.

Commonly observed fMRI responses to sustained stimulus feature transients, such as response adaptation (i.e. overshoot) during stimulation and post-stimulus undershoot after stimulus cessation (Bandettini et al., 1997; Frahm et al., 1996; Sadaghiani et al., 2009). These transients can be described by dynamic relationships between different physiological variables. While transients observed in the CBF response are usually directly related to the changes in excitatory-inhibitory (E-I) balance (Havlicek et al., 2015; Mullinger et al., 2013, 2014; Sadaghiani et al., 2009; Shmuel et al., 2006), transients observed in the BOLD responses (besides reflecting the contribution of the CBF transients) can additionally be caused by dynamic uncoupling between CBF and venous CBV (Buxton et al., 1998; Chen and Pike, 2009; Kim and Kim, 2011; Mandeville et al., 1999; Yacoub et al., 2006) or/and uncoupling between CBF and $CMRO_2$ (Donahue et al., 2009; Frahm et al., 2008; Lu et al., 2004; Poser et al., 2011; van Zijl et al., 2012).

During sustained (55 s long) stimulation using static and flickering checkerboards, we observed positive BOLD responses with fast initial increase followed by response adaptation, which was more pronounced in the response to static stimulus. This is in good agreement with previously reported results (Bandettini et al., 1997; Havlicek et al., 2015; Hoge et al., 1999). After stimulus cessation, the BOLD responses dipped quickly below baseline, exhibiting robust post-stimulus undershoots with long recovery period (~80 s), which is also commonly observed (Frahm et al., 1996; Krüger et al., 1996; van Zijl et al., 2012). In accordance with earlier results (Sadaghiani et al., 2009), the post-stimulus undershot after flickering stimulus was about twice as large as the post-stimulus undershoot after static stimulus (see Figs. 3 and 5). Furthermore, these transients were observed also in the CBF responses. However, the size of transients in the CBF responses was much smaller compared to those in the corresponding BOLD response (see also (Havlicek et al., 2015; Krüger et al., 1996)) and the post-stimulus deactivation after the static stimulus was almost negligible (similarly as indicated by (Sadaghiani et al., 2009)). Thus, these results suggest that the transients observed in the BOLD response can be only partly explained by the contribution from the CBF transients. The remaining contribution must be then attributed to the uncoupling between CBF and either venous CBV or/and $CMRO_2$, as discussed below.

Multi-TE sequences can provide additional functional information about physiological and physical sources underlying the BOLD signal (Poser and Norris, 2009; Posse, 2012; Posse et al., 1999). An approximately linear relationship between the fMRI signal amplitude and TE is expected for a GE sequence (Gati et al., 1997; Yacoub et al., 1999; Zhao et al., 2007a), which is largely dominated by the EV signal. Our multi-TE BOLD data were acquired at six regularly spaced TEs (in the range of 8–70 ms): the fractional change of BOLD response amplitude increased with TEs, in agreement with previous experimental results and theoretical predictions (e.g. (Donahue et al., 2011; Gati et al., 1997; Lu and Van Zijl, 2005; Menon et al., 1993; Uludağ et al., 2009; Yacoub et al., 2003)). However, the TE-dependence of the BOLD response during the early-overshoot and steady-state time-windows were sublinear, with small elevation between TE = 20–50 ms, and close to linear during the post-stimulus period (Fig. 4A). This was especially apparent after normalization with respect to the longest TE (Fig. 4B). Moreover, rather similar TE-dependencies were observed in the BOLD response transients and steady-state time-windows between the experimental conditions (see Fig. 4B).

After normalizing the BOLD responses acquired at different TEs with respect to the end of stimulation, it was further confirmed that the nonlinearity in TE-dependence is time-varying. These observations diverge from the common expectation that both steady-states and transient periods of the BOLD response have the same TE-dependence (Gati et al., 1997; Menon et al., 1993; Yacoub et al., 2003). This, together with the specific shape of a sublinear TE-dependence of the BOLD signal change mentioned above, suggests that at least during the positive response, there is a non-zero contribution of the nonlinearly TE-dependent IV signal change as described e.g. by Jin et al. (2006) and Zhao et al. (2007b). In contrast, a more linear TE-dependence during the post-stimulus undershoot (especially after static stimulus) suggests little or negligible contribution of the change in IV signal.

Linear regression analysis is usually applied to estimate the slope and intercept from TE-dependent fractional changes of BOLD data. The slope expresses the apparent ΔR_2^*, which is related to change in deoxyhemoglobin content, i.e. the BOLD effect. A non-zero intercept has been previously observed, which was typically attributed to non-BOLD effects – considered as erroneous signal possibly caused by inflow effects (Gao and Liu, 2012; Yacoub et al., 2003), changes in EV proton density (Stroman et al., 2002, 2003), head motion artifacts (Kundu et al., 2012), or an error from linear fitting to nonlinear TE-dependence (Jin et al., 2006). Moreover, both slope and intercept are usually evaluated only for signal change averaged over a specific time interval (Gati et al., 1997;

Yacoub et al., 2003; Zhao et al., 2007a). In our data, we have applied linear regression to every time-point of TE-dependent BOLD responses to estimate the slope and intercept time-courses. The calculated slope time-course closely resembled inverted BOLD response, featuring response characteristics such as early-undershoot and post-stimulus overshoot, with the same discrepancies between static and flickering conditions as observed in the BOLD responses (compare Figs. 4B and 5B). In contrast, the intercept had a very distinct time-course. The positive intercept response exhibited two distinct sequential phases after both stimulus onset and stimulus cessation (see Fig. 4B). A rapid increase and decrease occurred during the early stimulation phase and after stimulus cessation, respectively, which were followed by a slow increase (during stimulation) and return to baseline (after stimulus cessation, in ~100 s). The intercept responses obtained for static and flickering conditions had similar shape during the stimulation period but differed during the post-stimulus period. As argued below, the stronger post-stimulus undershoot observed in the CBF response after flickering stimulus reduces the value of the intercept, leading to a lower starting level of the slow return to baseline. Importantly, the shape of the intercept response is remarkably similar to the measured response of total CBV reported earlier by Mandeville et al. (1999) (see Fig. 3), where the fast and slow components of the response were described as the capillary (or arterial) CBV and venous CBV response contributions, respectively. Similarly distinct dynamics between arterial and venous CBV responses, were also observed by Kim and Kim (2011) (see Fig. 3b and c) or Huber et al. (2014a) (see Fig. 5b). Slower dynamics of the venous CBV with respect to CBF were also measured by (Chen and Pike, 2009; Kida et al., 2007). Accordingly, the slow return of the intercept (i.e. venous CBV in the interpretation of our data) to baseline can explain the presence of post-stimulus BOLD undershoot after static stimuli even with negligible post-stimulus undershoot in the CBF response (see Figs. 4B and 5A and B) (e.g. also in (Sadaghiani et al., 2009)). Therefore, one could speculate that the intercept time-courses estimated from TE-dependent BOLD data contain some information about physiologically meaningful variable, such as venous CBV. To further quantify the physiological origins of the intercept time-courses sources of TE-dependent nonlinearities mentioned above, theoretical simulations were employed.

4.1. Simulations

BOLD fMRI signal originates from both extravascular (EV) and intravascular (IV) components. Their relative contributions are weighted by CBV in various vascular compartments and are also dependent on the magnetic field strength, acquisition sequence and TE. At 1.5 T (or higher fields), while a linear TE-dependence of EV signal change is commonly observed (Donahue et al., 2011; Lu and Van Zijl, 2005), theoretical simulations suggest that the change in the IV signal is nonlinearly dependent on TE (Duong et al., 2003; Marques and Bowtell, 2006, 2008; Zhao et al., 2007b). The same simulations imply that the baseline IV-to-EV signal ratio, ε, is nonlinearly dependent on TE (see Fig. 1B for an example) and that for 3 T (or higher) and GE sequence, the contribution from IV signal change is reduced at longer TEs.

Simulations using two-compartment model of the BOLD signal were used before to demonstrate that the significant contribution of IV at shorter TEs can result in a non-zero intercept, because of linear fitting to the nonlinear TE-dependence of BOLD signal changes (Jin et al., 2006). To investigate the effect of the nonlinear TE-dependence of the IV signal on BOLD response transients and the shape of calculated intercept time-course, we have performed theoretical simulations using the two-compartmental BOLD signal model (Stephan et al., 2007) in conjunction with the dynamic balloon model (Buxton et al., 2004). The BOLD signal model allowed us to separate the linearly TE-dependent EV component from the nonlinearly TE-dependent IV and venous CBV components. Further, the balloon model allowed us to test two scenarios how the BOLD transients are caused (next to the variable CBF contribution), i.e. either by uncoupling of CBF-CBV (Scenario I) or CBF-$CMRO_2$ (Scenario II). Our simulation results showed that if we assume CBF response with the same size of signal change and transients as observed in the experimental CBF data, then both scenarios are capable to roughly reproduce the linear increase of the BOLD response amplitude with TE (see Fig. 3), including the size of the response transients. However, only CBF-CBV uncoupling reproduced both the expected increase of signal change with TE and the size of nonlinear time-varying TE-dependence of BOLD response transients after normalization (see Fig. 6 and Fig. S1). As a result, by applying a linear regression, both simulation scenarios provided similar slope time-courses, but only the TE-dependent BOLD data generated with CBF-CBV uncoupling yielded the positive intercept time-course comparable with the intercept obtained from the experimental data (compare Figs. 4B and 7B).

The size of the TE-dependent spread of signal amplitudes (well visible in normalized responses) during the overshoot and post-stimulus undershoot is mainly dictated by the TE-dependence of ε. However, the effect of ε on the TE-dependence of the response transients would be negligible if there is no uncoupling between CBF and venous CBV (data not shown). Similarly, if there is a strong CBF-CBV uncoupling, but ε is constant (i.e. TE-independent), then the effect size of TE-dependence of response transients is also minimal (data not shown). This means that conjunction of the CBF-CBV uncoupling and the nonlinear TE-dependence of ε is needed to reproduce the experimental data.

These results can be explained by analyzing components the BOLD signal equation (5). For voxels containing largely tissue parenchyma, the BOLD signal change is mainly dominated by the change in EV signal (see Fig. 1C) approximating a linear TE-dependence of the BOLD signal change. Therefore, the calculated slope explains the large range of signal changes between different TEs (for positive response, i.e. between ~0.5% and ~7%). The calculated intercept reflects signal changes that do not have a linear TE-dependence (i.e. having nonlinear TE-dependence due to ε – see below), such as changes in the IV and venous CBV signals. For 3 T and GE sequence, IV signal change is much smaller compared to EV signal change, with a peak (in our data <0.5%) between 20 and 50 ms (see Figs. S3 and S4). As the fMRI signal is dominated by the IV signal ($\varepsilon > 1$) at very short TEs (<25 ms) and by the EV signal ($\varepsilon < 1$) at longer TEs (>25 ms), the change in the venous CBV between two compartments is observed as positive at short TEs and negative at longer TEs (the profile of its TE-dependence is defined by ε). This means that the TE-dependence of the venous CBV signal change is different from the TE-dependence of the EV signal change but also from the IV signal change (see Figs. S3 and S4 for detailed illustration). Thus, a combination of these three components with distinct dynamic behaviors related to different physiological variables as described by Scenario I can explain the specific TE-dependences observed in the measured BOLD data during different time-windows and experimental conditions. For example, during steady-state the TE-dependence of BOLD response has the strongest deviation from a linear relationship (see Fig. 4B), because both IV and venous CBV signal changes are high due to activation (see Figs. S3 and S4). Therefore, their contribution causes an elevation in the TE-dependence of BOLD signal change between 20 and 50 ms and results in positive intercept that reflects both IV and venous CBF signal changes. On the other hand, during the post-stimulus undershoot, the IV signal change due to activation is negative and small (or negligible after the static stimulus), but, as the venous CBV is still elevated, it alters the dominant TE-dependence of EV signal. Thereby, the TE-dependence of the post-stimulus BOLD response undershoot appears more linear (especially for the static condition), but still results in a positive intercept (see Supplementary Material for more details). In contrast, Scenario II with a slow return of $CMRO_2$ to baseline during the post-stimulus period always results in a more negative change of the IV signal (see below for explanation) and the venous CBV follows the same dynamics as CBF (i.e. it is either very close to zero after the static stimulus or negative after the flickering stimulus). Therefore, only a negative signal change of the intercept response during post-stimulus period can be obtained by the Scenario II. Note that in the Supplementary Material, we provide a detailed reconstruction of the

BOLD signal TE-dependence only for Scenario I, as Scenario II is identified as implausible by examination of the BOLD signal equation (see below). In general, the intercept time-course represents a weighted sum of the IV and venous CBV signal changes, as described in Fig. 7C. As the direct contribution of IV and venous CBV signal changes to BOLD signal are small (given our voxel selection), the signal change of the intercept time-course is expected to be rather small, usually well below 1% (see Figs. 4B and 7B).

Given the identified contribution of physiological components to the calculated intercept from the theoretical BOLD signal model, the Scenario I with the CBF-CBV uncoupling is the most plausible explanation to the observed TE-dependence of BOLD response transients and specific shape of the intercept. The slow components in the intercept time-course (Fig. 4C) can only be obtained if we consider slower dynamics of venous CBV with respect to CBF. For almost complete return of CBF to baseline after stimulus ending and CBF-venous CBV uncoupling (i.e. Scenario I, static condition), the fractional changes in venous CBV and deoxyhemoglobin content are nearly identical (see Fig. 6A) and, thus, the IV signal change (i.e. the second term in Eq. (5)) is close to zero. In this case, the post-stimulus intercept time-course almost exclusively represents venous CBV. The fast intercept components are dominated by the IV signal change (inversely related to the deoxyhemoglobin concentration), whose time-course is by its shape comparable to CBF (or arterial CBV) response; i.e. the more pronounced transients seen in the deoxyhemoglobin content are removed by division with venous CBV (see Fig. 7C). In the Scenario II, $CMRO_2$ (with slower dynamics compared to the CBF) has only an indirect contribution to the intercept via the IV signal change. The venous CBV is, in this case, approximately just a scaled version of the CBF response. Therefore, if we divide the deoxyhemoglobin content that already has pronounced transients (due to CBF-$CMRO_2$ uncoupling) by venous CBV, these transients are even more emphasized, resulting in the intercept time-course with similar transients as the BOLD response. This means that the hypothesis of CBF-$CMRO_2$ uncoupling being the cause of the BOLD response transient cannot produce a time-varying non-linear TE dependence and an intercept response that is compatible with our experimental observations. Thus, the BOLD signal equation provides a direct proof that Scenario II is implausible.

We have also evaluated the possibility that both CBV and $CMRO_2$ are uncoupled from CBF (see Fig. S2). These simulations showed that already a small contribution of CBF-$CMRO_2$ uncoupling leads to a significant decrease of the intercept response to flickering stimulus below baseline during the post-stimulus undershoot and to an early-overshoot in the intercept positive response to static stimulus, which is not comparable with the experimental observations. Therefore, even though we cannot completely rule out any contribution of CBF-$CMRO_2$ uncoupling to BOLD response transients, the dominant source of the contribution to the transients (not already covered by CBF transients) is CBF-CBV uncoupling.

Furthermore, considering two experimental conditions played an important role in testing two physiological scenarios. As the CBF responses to static and flickering stimuli exhibited strong differences in the response transients, i.e. in response adaptation and the size of the post-stimulus undershoot, we were able to simulate and control the variable CBF contribution to the BOLD response transients. Since the CBF response to static stimulus had an almost negligible post-stimulus undershoot, we can conclude that in this case the BOLD response undershoot almost exclusively results from a CBF-CBV uncoupling (i.e. post-stimulus intercept response reflects venous CBV). The CBF response to flickering stimulus showed a stronger post-stimulus undershoot that significantly contributes to the size of post-stimulus BOLD undershoot. As CBF and $CMRO_2$ are tightly coupled, there is, in this case, a direct contribution of $CMRO_2$ to the BOLD response undershoot (see Fig. S1). However, also in this case (and as we showed in Fig. S2B), the larger part of post-stimulus BOLD undershoot is due to CBF-CBV uncoupling (i.e. post-stimulus intercept response reflects both IV and venous CBV signal changes). This explains why we see significant differences in the post-stimulus intercept time-courses after the static and flickering stimuli (see Fig. 4C) and why there is slightly more nonlinearity present in the TE-dependence profile of the BOLD response undershoot after the flickering stimulus compared to the static stimulus (see Fig. 4B). None of these can be predicted if CBF-$CMRO_2$ uncoupling is the dominant cause of the BOLD signal transients.

In summary, the TE-dependence of the BOLD response transients provides a strong evidence that the BOLD transients, such as overshoot and post-stimulus undershoot, are the result of neuronal mechanisms reflected in coupled CBF-$CMRO_2$ responses (Krüger et al., 1996; Mullinger et al., 2014; Sadaghiani et al., 2009) and vascular mechanism related to delayed compliance of venous vessels (Chen and Pike, 2009; Huber et al., 2014a; Kida et al., 2007; Kim and Ogawa, 2012; Mandeville et al., 1999; Yacoub et al., 2006). Moreover, it provides a strong argument against the hypothesis that the BOLD response transients are mainly due to a slower dynamics of the $CMRO_2$ response with respect to CBF, as suggested by, for example ((Frahm et al., 2008; Hua et al., 2011; Poser et al., 2011; van Zijl et al., 2012) and references therein).

4.2. Limitations and recommendations

The shape and amplitude of the calculated intercept can be potentially affected by several factors: the composition of selected voxels, the number and the range of TEs, the field strength and the acquisition sequence.

In our study, we aimed to select activated voxels within tissue parenchyma of gray matter. However, with 3 mm isotropic voxel size, some partial-voluming with other tissue types cannot be completely avoided. To minimize its effects, we only considered voxels, whose estimated T_2^* values laid within a narrow range (±5 ms) around the main distribution peak at ~ 47 ms that was earlier identified as (susceptibility artifact-free) tissue-T_2^* at 3 T (see e.g. (Lu and Van Zijl, 2005; Triantafyllou et al., 2011)). Selected voxels showed large overlap with the CBF activation map (see Table S1). Since CBF activation maps are more localized to the site of neuronal activation than BOLD maps ((Liu and Brown, 2007) and references therein), and large CBF response (~80% in our data) are not found in CSF and white matter, it confirms that the selected set of BOLD signal voxels indeed mainly belong to gray matter. Moreover, as a large number of voxels (~140 per subject) were averaged based on above-mentioned criteria, the partial volume effects are expected to be minimal. Note that by selecting a broader window, we would increase the number of voxels with possibly higher content of larger vein structures or partial voluming with white matter or CSF. In the former case, we expect changes in the baseline IV-to-EV signal ratio due to a stronger contribution of the IV signal change (and possible inflow effect – see below) to the BOLD signal at 3 T, resulting in a different shape and scaling of the intercept time-course as the relative contribution of IV and venous CBV signal changes is altered. In the latter case, significant partial voluming with white matter or CSF voxels can introduce additional nonlinearities into the TE-dependence. Furthermore, activity dependent changes in T1 and CSF were reported before (Donahue et al., 2006; Huber et al., 2016; Jin and Kim, 2010; Piechnik et al., 2009; Renvall et al., 2014; Scouten and Constable, 2008). These changes are due to blood volume changes in the IV compartments (and consequent enlargement of gray matter that alters voxels' partial volume). In this work, we ignore these secondary changes and their possible contributions to the intercept time-course, and rather focus on modeling the primary changes in the EV and IV compartments. Thus, future research has to quantify the effect of these contributions on the intercept time-course.

A non-zero intercept was before attributed also to other possible sources such as inflow effect, change in EV water proton density, or head motion related artifacts (e.g. (Gao and Liu, 2012; Kundu et al., 2012;

Stroman et al., 2001, 2003; Yacoub et al., 2003)). The inflow effect is caused by fresh spins flowing from outside the slice into the voxel, thereby replacing the saturated spins and causing a faster recovery of the longitudinal magnetization. The magnitude of this inflow effect is known to be significant in large vessels (arteries and veins) and it decreases with increasing TR (and/or lowering the flip-angle (Gonzalez-castillo et al., 2011; Lu et al., 2002)). Further, it was observed that the inflow effect adds a faster component to the BOLD response (Liu and Buckle, 2008). In our study, we used voxels mainly attributed to gray matter, where the inflow effect is known to be minimal even with short TR (Lu et al., 2002), and acquired data with relatively long TR = 3.3 s, which also significantly reduces the inflow effect. Nevertheless, it is important to realize that if we assume a small contribution of inflow present in large veins (e.g. 2% veins and 0.8% arteries in tissue parenchyma as assumed previously (Lu et al., 2002; Zhao et al., 2007b)), then this contribution is already reflected in modeled IV signal change. In other words, the inflow effect can modulate the relative contribution of IV signal change and the TE-dependence of baseline IV-to-EV signal ratio, ε. This means, that a contribution of inflow effect in venous vessels, even though minimal in our data, does not change interpretation of our results, as it is part of the modeled IV signal change.

The suggestion that the positive intercept is due to increase of EV water proton density during activation was later disproven by other results (Jin et al., 2006; Jochimsen et al., 2005; Yacoub et al., 2003), as the positive intercept disappeared after applying diffusion weighting eliminating IV signal contribution (but also any possible contribution of the inflow effect). That is, if the positive intercept is due to increase of EV proton density, then it should remain unaffected by diffusion weighting. The intercept related to head motion artifact is characterized by spatially structured artifacts with higher frequency content than the hemodynamic response (Kundu et al., 2012). Other sources, such as errors in estimated TEs can result in non-zero intercept (Dymerska et al., 2016; Goense and Logothetis, 2006) as well. TEs reported in the current study, which refer to TE at the center of the *k*-space, differed negligibly from the effective TEs (Deichmann et al., 2002, 2003), with differences well within 1 ms. In general, any systematic scaling of TEs will not affect the shape of intercept time-course, but only its scaling.

Importantly, we were able to provide an accurate description of the intercept time-course using an established theoretical model that does not include any of the aforementioned sources. Thus, even though contributions from other sources cannot be completely excluded, they are not necessary to explain the experimental observations, as the specific shape of the intercept time-course with distinct transients can be reconciled with the observed BOLD or CBF responses combined with a well-established theoretical model of the BOLD signal. By saying that, recent developments in VASO fMRI techniques that allow measuring CBV in both arterial and venous compartments (Huber et al., 2014a, 2014b) could be employed to quantitatively validate our modeling results and interpretation of the intercept time-course.

We calculated the slope and intercept from multi-TE data consisting of six regularly spaced TEs between 8 ms and 70 ms. This relatively high number of echoes and sufficiently large range at 3 T (and averaging over many voxels and trials) ensures robust estimates of the slope and intercept. The effect of nonlinearity of the IV signal on the intercept is TE-dependent, which means that for different TEs, the intercept is formed with different weighting of signal changes in the IV and venous CBV components (see Fig. 7C). However, our additional simulations showed (see Fig. S5) that, in the ideal case of constant CNR across TEs, the main features of the intercept time-course (i.e. the relative contribution of IV and venous CBV signal changes remain approximately constant) are preserved, if we effectively cover the range of nonlinear TE-dependence (e.g. between 20 and 60 ms). Nevertheless, the number of TEs influences the scale of the intercept. In other words, in this ideal case, even with only two TEs one should obtain a similar shape of the intercept time-course. However, the CNR is not constant across TEs (see Fig. S6), and for our TE range, it exhibits a typical inverted U-shape (Poser et al., 2006; Posse et al., 1999) with the lowest CNR scored by the shortest TE (8 ms). Therefore, to reliably estimate the intercept, one should try to balance the CNR between lower and higher TEs. This is easier to achieve if data at more than two TEs are acquired. In our case, data provided by the lowest TE is noisy and therefore less reliable, however, our other five TEs compensate for this. Therefore, we obtain almost identical intercept time-course even if we only use the later five TEs (data not shown). Note that we have achieved reasonably good CNR across different TEs by averaging over larger set of voxels and trials. As the reliability of intercept estimate (with expected signal change < 1%) depends crucially on the CNR at different TEs, intercept time-course estimates based on single or very few voxels and/or small number of trails, and/or TEs with unbalanced CNRs will not be reliable and less comparable with the predictions of the theoretical model. In this paper, we provided the theoretical model and CNR curves (Fig. S6), which can be used together to optimize the number and range of ideal TEs in order to reliably estimate the intercept time-course (at 3 T and using GE sequence).

The fast component of intercept time-course is determined by the IV signal change, which is dependence on TE, field strength and acquisition sequence. While the EV signal change contribution is expected to increase with both TE and B_0, the amount of IV signal change decreases (Duong et al., 2003; Lu and Van Zijl, 2005; Uludağ et al., 2009; Yacoub et al., 2003). In general, the contribution of IV signal to the BOLD response is lower for GE compared to spin-echo (SE) contrast at longer TEs (Uludağ et al., 2009; Zhao et al., 2007b). That is because for GE and 3 T the contribution of IV signal change is significant at lower TEs but diminishes with increasing TE for values exceeding the blood T_2^*, whereas T_2 of blood is longer, hence the IV signal contribution is high also at longer TEs. As with higher fields, T_2^* and T_2 become shorter, the expected 'bump' in TE-dependence of IV signal change moves towards shorter TEs. Therefore, the amount/presence of nonlinearity in TE-dependence of BOLD signal due to IV signal changes depends on the field strength, MR sequence and the range of sampled TEs. If there is significant contribution of IV signal change, the intercept at TE = 0 ms is likely to reflect both IV signal and venous CBV changes. However, if the contribution of IV signal is negligible (i.e. ε is close to zero), the effect of the blood volume change becomes TE-independent and we expect to obtain an intercept reflecting negative change caused by the blood volume (i.e. due to blood volume decrease in the EV compartment, which is the VASO effect (Huber et al., 2014b; Lu et al., 2003)).

In this study, the experimental observations are explained using a two-compartment model of the BOLD signal that distinguishes EV and IV signal contributions, and accounts for the dynamic interplay between the underlying physiological variables using the balloon model (Buxton et al., 1998; Havlicek et al., 2015). As mentioned above, including the change in IV signal into the model is essential for studying the TE-dependence of the BOLD response. In this sense, utilization of simpler models (Davis et al., 1998; Obata et al., 2004) that ignore IV signal component is not appropriate. The IV signal itself contains contributions from all vessel sizes: i.e. arteries, arterioles, capillaries, venules and veins (Uludağ et al., 2009). However, at 3 T using GE sequence, the BOLD signal is dominated by the signal from the venous compartments (represented mainly by the post-capillary venules and ascending veins as large pial veins were mostly avoided by our voxel selection criteria), supporting our choice of the BOLD signal model with a single IV compartment. Further, the IV signal is affected by chemical exchange of water molecules between plasma and red blood cells and by the diffusion of plasma water in the presence of magnetic field gradients generated by deoxyhemoglobin (Duong et al., 2003), which makes the IV signal change nonlinearly dependent on TE (with a clear bump between 20 and 50 ms in case of GE sequence at 3 T). This chemical exchange/diffusion can be described by the Luz-Meiboom model (Brooks, 2002; Luz and

Meiboom, 1963; Stefanovic and Pike, 2004). Although this model is not directly included in our theoretical simulations, the assumed (nonlinear) TE-dependence of baseline IV-to-EV signal ratio, ϵ (see Fig. 1B), is closely motivated by the simulation results generated by this model (Duong et al., 2003). Next, utilization of the dynamic balloon model (Buxton et al., 1998) is crucial for interpreting the dynamic relationships between different physiological parameters and necessary to study the physiological origins of BOLD response transients. Thus, further improvements of current modeling could include multiple vascular comportments and partial voluming with white matter and CSF. However, the extension of the current BOLD signal model with these contributions can only be evaluated, if additional experimental data is acquired to quantify them.

Although we showed simulations only for specific set of model parameter values within physiologically reasonable ranges (Supplementary Material), these values were carefully selected based on a systematic grid-search procedure to exclude the possibility that there is a parameter combination for which both scenarios can reproduce the experimental data. Moreover, for CBF-CBV uncoupling (i.e. Scenario I), a broader range of α and n values can provide a good approximation to observed TE-dependence of BOLD response transients in the experimental data. Importantly, simulations used in this study were mainly meant to provide an illustration, not a proof, of the plausibility of the two physiological scenarios (or their combinations). The proof itself is given by the fact that the experimental observations – such as the time-varying nonlinear TE dependence and slow return of the positive post-stimulus intercept to baseline – are only properly described by the nonlinearly TE-dependent BOLD signal equation (5) in conjunction with a CBF-CBV uncoupling.

In this study, we have used relatively long stimulus duration (55 s). As the venous CBV steadily increases during stimulation due to viscoelasticity of venous vessels and then slowly returns to baseline due to the same mechanism, its contribution to the BOLD response transients become more dominant with longer stimuli ((Uludag and Blinder, 2017), and references therein). It has been hypothesized that the size of CBF-CBV uncoupling is proportional to the stimulus duration. The full recovery from the post-stimulus BOLD undershoot can take twice or more as long as the stimulus duration. This means that our results about CBF-CBV uncoupling being dominant mechanism behind the post-stimulus BOLD undershoot (in addition to a variable CBF contribution) should also be scalable to shorter stimuli. However, in the case of very short stimuli (e.g. < 5 s), this extrapolation might not hold anymore and other physiological mechanisms may take over. By saying that, multi-TE sequence could be useful to provide insights into physiological mechanisms in this case as well.

Acknowledgements

This work was financially supported by a VIDI grant (#452-11-002) of the Netherlands Organization for Scientific Research (NWO) to KU. We would also like to thank the three reviewers for their invaluable help in presenting this work rigorously and clearly.

Appendix A. Supplementary data

Supplementary data related to this article can be found at http://dx.doi.org/10.1016/j.neuroimage.2017.07.034.

References

Bandettini, P.A., Kwong, K.K., Davis, T.L., Tootell, R.B.H., Wong, E.C., Fox, P.T., Belliveau, J.W., Weisskoff, R.M., Rosen, B.R., 1997. Characterization of cerebral blood oxygenation brain activation, 109, 93–109.

Barth, M., Metzler, A., Klarhöfer, M., Röll, S., Moser, E., Leibfritz, D., 1999. Functional MRI of the human motor cortex using single-shot, multiple gradient-echo spiral imaging. Magn. Reson Imaging 17, 1239–1243.

Barth, M., Windischberger, C., Klarhöfer, M., Moser, E., 2001. Characterization of BOLD activation in multi-echo fMRI data using fuzzy cluster analysis and a comparison with quantitative modeling. NMR Biomed. 14, 484–489.

Boxerman, J.L., Bandettini, P.A., Kwong, K.K., Baker, J.R., Davis, T.L., Rosen, B.R., Weisskoff, R.M., 1995. The intravascular contribution to fMRI signal change: monte Carlo modeling and diffusion-weighted studies in vivo. Magnetic Reson. Med. 34, 4–10.

Brooks, R.A., 2002. T2 -shortening by strongly magnetized spheres: a chemical exchange model, 391, 388–391.

Buxton, R.B., 2001. The elusive initial dip. NeuroImage 13, 953–958.

Buxton, R.B., Frank, L.R., 1997. A model for the coupling between cerebral blood flow and oxygen metabolism during neural stimulation. J. Cereb. Blood Flow Metab 17, 64–72.

Buxton, R.B., Uludag, K., Dubowitz, D.J., Liu, T.T., 2004. Modeling the hemodynamic response to brain activation. NeuroImage 23, S220–S233. ST - Modeling the hemodynamic response.

Buxton, R.B., Wong, E.C., Frank, L.R., 1998. Dynamics of blood flow and oxygenation changes during brain activation: the balloon model. Magnetic Reson. Med. 39, 855–864. ST - Dynamics of blood flow and oxygenati.

Chen, J.J., Pike, G.B., 2009. Origins of the BOLD post-stimulus undershoot. NeuroImage 46, 559–568.

Cheng, Y., van Zijl, P.C.M., Hua, J., 2015. Measurement of parenchymal extravascular R2* and tissue oxygen extraction fraction using multi-echo vascular space occupancy MRI at 7T. NMR Biomed. 28, 264–271.

Davis, T.L., Kwong, K.K., Weisskoff, R.M., Rosen, B.R., 1998. Calibrated functional MRI: mapping the dynamics of oxidative metabolism. Proc. Natl. Acad. Sci. U. S. A. 95, 1834–1839.

Deichmann, R., Gottfried, J.A., Hutton, C., Turner, R., 2003. Optimized EPI for fMRI studies of the orbitofrontal cortex, 19, 430–441.

Deichmann, R., Josephs, O., Hutton, C., Corfield, D.R., Turner, R., 2002. Compensation of susceptibility-induced BOLD sensitivity losses in echo-planar fMRI imaging, 135, 120–135.

Donahue, M.J., Hoogduin, H., Van Zijl, P.C.M., Jezzard, P., Luijten, P.R., Hendrikse, J., 2011. Blood oxygenation level-dependent (BOLD) total and extravascular signal changes and ΔR2* in human visual cortex at 1.5, 3.0 and 7.0 T. NMR Biomed. 24, 25–34.

Donahue, M.J., Lu, H., Jones, C.K., Edden, R.A.E., Pekar, J.J., Zijl, P.C.M.V., 2006. Theoretical and experimental investigation of the VASO contrast mechanism. Magnetic Reson. Med. 1273, 1261–1273.

Donahue, M.J., Stevens, R.D., de Boorder, M., Pekar, J.J., Hendrikse, J., van Zijl, P.C.M., 2009. Hemodynamic changes after visual stimulation and breath holding provide evidence for an uncoupling of cerebral blood flow and volume from oxygen metabolism. J. Cereb. Blood Flow Metabol. Off. J. Int. Soc. Cereb. Blood Flow Metabol. 29, 176–185.

Duong, T.Q., Yacoub, E., Adriany, G., Hu, X., Uğurbil, K., Kim, S.G., 2003. Microvascular BOLD contribution at 4 and 7 T in the human brain: gradient-echo and spin-echo fMRI with suppression of blood effects. Magnetic Reson. Med. 49, 1019–1027.

Dymerska, B., Cardoso, P., Mahr, N., Matt, E., Fischmeister, F., Beisteiner, R., Trattnig, S., Robinson, S.D., 2016. Investigating the Impact of Temporal Signal Fluctuations and Local Effective Echo Times on Indices of BOLD Sensitivity in Healthy Subjects and Tumor Patients at 7T. ISMRM, Singapore, 0221–0221.

Frahm, J., Baudewig, J., Kallenberg, K., Kastrup, A., Merboldt, K.D., Dechent, P., 2008. The post-stimulation undershoot in BOLD fMRI of human brain is not caused by elevated cerebral blood volume. NeuroImage 40, 473–481.

Frahm, J., Krüger, G., Merboldt, K.D., Kleinschmidt, A., 1996. Dynamic uncoupling and recoupling of perfusion and oxidative metabolism during focal brain activation in man. Magnetic Reson. Med. Off. J. Soc. Magnetic Reson. Med./Soc. Magnetic Reson. Med. 35, 143–148.

Gao, J.-H., Liu, H.-L., 2012. Inflow effects on functional MRI. NeuroImage 62, 1035–1039.

Gati, J.S., Menon, R.S., Uğurbil, K., Rutt, B.K., 1997. Experimental determination of the BOLD field strength dependence in vessels and tissue. Magnetic Reson. Med. 38, 296–302.

Goense, J.B.M., Logothetis, N.K., 2006. Laminar specificity in monkey V1 using high-resolution SE-fMRI. Magn. Reson. Imaging 24, 381–392.

Gonzalez-castillo, J., Roopchansingh, V., Bandettini, P.A., Bodurka, J., 2011. Physiological noise effects on the flip angle selection in BOLD fMRI. NeuroImage 54, 2764–2778.

Griffeth, V.E.M., Blockley, N.P., Simon, A.B., Buxton, R.B., 2013. A new functional MRI approach for investigating modulations of brain oxygen metabolism. PLoS ONE 8 e68122–e68122.

Griffeth, V.E.M., Buxton, R.B., 2011. A theoretical framework for estimating cerebral oxygen metabolism changes using the calibrated-BOLD method: modeling the effects of blood volume distribution, hematocrit, oxygen extraction fraction, and tissue signal properties on the BOLD signal. NeuroImage 58, 198–212.

Griswold, M.A., Jakob, P.M., Heidemann, R.M., Nittka, M., Jellus, V., Wang, J., Kiefer, B., Haase, A., 2002. Generalized autocalibrating partially parallel acquisitions (GRAPPA). Magnetic Reson. Med. 47, 1202–1210.

Grubb, R.L., Raichle, M.E., Eichling, J.O., Ter-Pogossian, M.M., 1974. The effects of changes in PaCO2 cerebral blood volume, blood flow, and vascular mean transit time. Stroke 5, 630–639.

Havlicek, M., Roebroeck, A., Friston, K., Gardumi, A., Ivanov, D., Uludag, K., 2015. Physiologically informed dynamic causal modeling of fMRI data. NeuroImage 122, 355–372.

Havlicek, M., Roebroeck, A., Friston, K.J., Gardumi, A., Ivanov, D., Uludag, K., 2017. On the importance of modeling fMRI transients when estimating e ff ective connectivity: a dynamic causal modeling study using ASL data. NeuroImage 155, 217–233.

Hernandez-Garcia, L., Jahanian, H., Rowe, D.B., 2010. Quantitative analysis of arterial spin labeling FMRI data using a general linear model. Magn. Reson. Imaging 28, 919–927.

Hoge, R.D., Atkinson, J., Gill, B., Crelier, G.R., Marrett, S., Pike, G.B., 1999. Stimulus-dependent BOLD and perfusion dynamics in human V1. NeuroImage 9, 573–585.
Hua, J., Stevens, R.D., Huang, A.J., Pekar, J.J., Zijl, P.C.M.V., 2011. Physiological origin for the BOLD poststimulus undershoot in human brain: vascular compliance versus oxygen metabolism. J. Cereb. Blood Flow Metabol. 31, 1599–1611.
Huber, L., Goense, J., Kennerley, A.J., Ivanov, D., Krieger, S.N., Lepsien, J., Trampel, R., Turner, R., Möller, H.E., 2014a. Investigation of the neurovascular coupling in positive and negative BOLD responses in human brain at 7T. NeuroImage 97, 349–362.
Huber, L., Ivanov, D., Krieger, S.N., Streicher, M.N., Mildner, T., Poser, B.A., Möller, H.E., Turner, R., 2014b. Slab-selective, BOLD-corrected VASO at 7 Tesla provides measures of cerebral blood volume reactivity with high signal-to-noise ratio. Magnetic Reson. Med. Off. J. Soc. Magnetic Reson. Med./Soc. Magnetic Reson. Med. 72, 137–148.
Huber, L., Marrett, S., Handwerker, D.A., Thomas, A., Gutierrez, B., Ivanov, D., Poser, B.A., Bandettini, P.A., 2016. Fast Dynamic Measurement of Functional T1 and Grey Matter Thickness Changes during Brain Activation at 7T. Singapore, 0633–0633.
Jin, T., Kim, S.-G., 2010. Change of the cerebrospinal fluid volume during brain activation investigated by T1ρ-weighted fMRI. NeuroImage 51, 1378–1383.
Jin, T., Wang, P., Tasker, M., Zhao, F., Kim, S.-g., 2006. Source of nonlinearity in echo-time-dependent BOLD fMRI. Magnetic Reson. Med. 1290, 1281–1290.
Jochimsen, T.H., Norris, D.G., Möller, H.E., 2005. Is there a change in water proton density associated with functional magnetic resonance imaging? Magnetic Reson. Med. 53, 470–473.
Kida, I., Rothman, D.L., Hyder, F., 2007. Dynamics of changes in blood flow, volume, and oxygenation: implications for dynamic functional magnetic resonance imaging calibration. J. Cereb. Blood Flow Metabol. Off. J. Int. Soc. Cereb. Blood Flow Metabol. 27, 690–696.
Kim, S.-G., 1995. Quantification of relative cerebral blood flow change by flow-sensitive alternating inversion recovery (FAIR) technique: application to functional mapping. Magnetic Reson. Med. 34, 293–301.
Kim, S.-G., Ogawa, S., 2012. Biophysical and physiological origins of blood oxygenation level-dependent fMRI signals. J. Cereb. Blood Flow Metabol. Off. J. Int. Soc. Cereb. Blood Flow Metabol. 32, 1188–1206.
Kim, T., Kim, S.-G., 2011. Temporal dynamics and spatial specificity of arterial and venous blood volume changes during visual stimulation: implication for BOLD quantification. J. Cereb. Blood Flow Metabol. Off. J. Int. Soc. Cereb. Blood Flow Metabol. 31, 1211–1222.
Krüger, G., Fransson, P., Merboldt, K.D., Frahm, J., 1999. Does stimulus quality affect the physiologic MRI responses to brief visual activation? Neuroreport 10, 1277–1281.
Krüger, G., Kleinschmidt, A., Frahm, J., 1996. Dynamic MRI sensitized to cerebral blood oxygenation and flow during sustained activation. Magnetic Reson. Med. 35, 797–800.
Kundu, P., Benson, B.E., Baldwin, K.L., Rosen, D., Luh, W.M., Bandettini, P.A., Pine, D.S., Ernst, M., 2015. Robust resting state fMRI processing for studies on typical brain development based on multi-echo EPI acquisition. Brain Imaging Behav. 9, 56–73.
Kundu, P., Brenowitz, N.D., Voon, V., Worbe, Y., Vértes, P.E., Inati, S.J., Saad, Z.S., Bandettini, P.A., Bullmore, E.T., 2013. Integrated strategy for improving functional connectivity mapping using multiecho fMRI. Proc. Natl. Acad. Sci. Unites States Am. 110, 16187–16192.
Kundu, P., Inati, S.J., Evans, J.W., Luh, W.-M., Bandettini, P.A., 2012. Differentiating BOLD and non-BOLD signals in fMRI time series using multi-echo EPI. NeuroImage 60, 1759–1770.
Lee, S.-p.P., Silva, A.C., Ugurbil, K., Kim, S.-G.G., 1999. Diffusion-weighted spin-echo fMRI at 9.4T: microvascular/tissue contribution to BOLD signal changes. Magnetic Reson. Med. 928, 919–928.
Liu, H.-l., Buckle, C., 2008. Inflow effects on hemodynamic responses characterized by event-related f MRI using gradient-echo EPI sequences. Med. Phys. 35, 4301–4307.
Liu, T.T., Brown, G.G., 2007. Measurement of cerebral perfusion with arterial spin labeling : Part 1. Methods. J. Int. Neuropsychol. Soc. 13, 517–525.
Liu, T.T., Wong, E.C., Frank, L.R., Buxton, R.B., 2002. Analysis and design of perfusion-based event-related fMRI experiments. NeuroImage 16, 269–282.
Lu, H., Golay, X., Pekar, J.J., Van Zijl, P.C.M., 2003. Functional magnetic resonance imaging based on changes in vascular space occupancy. Magnetic Reson. Med. 50, 263–274.
Lu, H., Golay, X., Pekar, J.J., Van Zijl, P.C.M., 2004. Sustained poststimulus elevation in cerebral oxygen utilization after vascular recovery. J. Cereb. Blood Flow Metabol. Off. J. Int. Soc. Cereb. Blood Flow Metabol. 24, 764–770.
Lu, H., Golay, X., Zijl, P.C.M.V., 2002. Intervoxel heterogeneity of event-related functional magnetic resonance imaging responses as a Function of T 1 weighting, 955, 943–955.
Lu, H., Van Zijl, P.C.M., 2005. Experimental measurement of extravascular parenchymal BOLD effects and tissue oxygen extraction fractions using multi-echo VASO fMRI at 1.5 and 3.0 T. Magnetic Reson. Med. 53, 808–816.
Luz, Z., Meiboom, S., 1963. Nuclear magnetic resonance study of the protolysis of trimethylammonium ion in aqueous solution—order of the reaction with respect to solvent. J. Chem. Phys. 39, 366–366.
Mandeville, J.B., Marota, J.J., Kosofsky, B.E., Keltner, J.R., Weissleder, R., Rosen, B.R., Weisskoff, R.M., 1998. Dynamic functional imaging of relative cerebral blood volume during rat forepaw stimulation. Magnetic Reson. Med. Off. J. Soc. Magnetic Reson. Med./Soc. Magnetic Reson. Med. 39, 615–624.
Mandeville, J.B., Marota, J.J.A., Ayata, C., Zaharchuk, G., Moskowitz, M.A., Rosen, B.R., Weisskoff, R.M., 1999. Evidence of a cerebrovascular postarteriole windkessel with delayed compliance. J. Cereb. Blood Flow Metabol. 19, 679–689 (ST - Evidence of a cerebrovascular postar).
Marques, J.P., Bowtell, R.W., 2004. Simulations of the BOLD effect using a realistic model of the vasculature, 11, 2004–2004.
Marques, J.P., Bowtell, R.W., 2006. Understanding the intra- and extravascular contributions to the BOLD effect through simulations. Proc. Int. Soc. Magnetic Reson. Med. 14, 896–896.
Marques, J.P., Bowtell, R.W., 2008. Using forward calculations of the magnetic field perturbation due to a realistic vascular model to explore the BOLD effect. NMR Biomed. 21, 553–565.
Menon, R.S., Ogawa, S., Tank, D.W., Ugurbil, K., 1993. 4 tesla gradient recalled echo characteristics of photic stimulation-induced signal changes in the human primary visual cortex. Magnetic Reson. Med. 30, 380–386.
Mugler, J.P., Brookeman, J.R., 1990. Three-dimensional magnetization-prepared rapid gradient-echo imaging (3D MP RAGE). Magnetic Reson. Med. 15, 152–157.
Mullinger, K.J., Mayhew, S.D., Bagshaw, A.P., Bowtell, R., Francis, S.T., 2013. Poststimulus Undershoots in Cerebral Blood Flow and BOLD FMRI Responses Are Modulated by Poststimulus Neuronal Activity.
Mullinger, K.J., Mayhew, S.D., Bagshaw, A.P., Bowtell, R., Francis, S.T., 2014. Evidence that the negative BOLD response is neuronal in origin: a simultaneous EEG-BOLD-CBF study in humans. NeuroImage 94, 263–274.
Mumford, J.a., Hernandez-Garcia, L., Lee, G.R., Nichols, T.E., 2006. Estimation efficiency and statistical power in arterial spin labeling fMRI. NeuroImage 33, 103–114.
Obata, T., Liu, T.T., Miller, K.L., Luh, W.M., Wong, E.C., Frank, L.R., Buxton, R.B., 2004. Discrepancies between BOLD and flow dynamics in primary and supplementary motor areas: application of the balloon model to the interpretation of BOLD transients. NeuroImage 21, 144–153. ST - Discrepancies between BOLD and flow.
Ogawa, S., Lee, T.M., Kay, A.R., Tank, D.W., 1990. Brain magnetic resonance imaging with contrast dependent on blood oxygenation. Proc. Natl. Acad. Sci. 87, 9868–9872.
Ogawa, S., Menon, R.S., Tank, D.W., Kim, S.G., Merkle, H., Ellermann, J.M., Ugurbil, K., 1993. Functional brain mapping by blood oxygenation level-dependent contrast magnetic resonance imaging. A comparison of signal characteristics with a biophysical model. Biophysical J. 64, 803–812.
Peltier, S., 2002. T2* dependence of low frequency functional connectivity. NeuroImage 16, 985–992.
Piechnik, S.K., Evans, J., Bary, L.H., Wise, R.G., Jezzard, P., 2009. Functional changes in CSF volume estimated using measurement of water T 2 relaxation, 586, 579–586.
Poser, B.A., Mierlo, E.V., Norris, D.G., 2011. Exploring the post-stimulus undershoot with spin-echo fMRI: implications for models of neurovascular response, 153, 141–153.
Poser, B.a., Norris, D.G., 2009. Investigating the benefits of multi-echo EPI for fMRI at 7 T. NeuroImage 45, 1162–1172.
Poser, B.A., Versluis, M.J., Hoogduin, J.M., Norris, D.G., 2006. BOLD contrast sensitivity enhancement and artifact reduction with multiecho EPI: parallel-acquired inhomogeneity-desensitized fMRI. Magnetic Reson. Med. 55, 1227–1235.
Posse, S., 2012. Multi-echo acquisition. NeuroImage 62, 665–671.
Posse, S., Wiese, S., Gembris, D., Mathiak, K., Kessler, C., Grosse-Ruyken, M.L., Elghahwagi, B., Richards, T., Dager, S.R., Kiselev, V.G., 1999. Enhancement of BOLD-contrast sensitivity by single-shot multi-echo functional MR imaging. Magnetic Reson. Med. 42, 87–97.
Renvall, V., Witzel, T., Bianciardi, M., Polimeni, J.R., 2014. Multi-contrast inversion-recovery EPI (MI-EPI) functional MRI at 7 T. ISMRM 22, 14075–14075.
Sadaghiani, S., Uğurbil, K., Uludağ, K., 2009. Neural activity-induced modulation of BOLD poststimulus undershoot independent of the positive signal. Magn. Reson. Imaging 27, 1030–1038.
Scouten, A., Constable, R.T., 2008. VASO-based calculations of CBV change. Account. Dyn. CSF Volume 315, 308–315.
Shmuel, A., Augath, M., Oeltermann, A., Logothetis, N.K., 2006. Negative functional MRI response correlates with decreases in neuronal activity in monkey visual area. Nat. Neurosci. 9, 569–577, V1. .
Speck, O., Hennig, J., 1998. Functional Imaging by I0- and T2* -parameter mapping using multi-image EPI. Magnetic Reson. Med. 40, 243–248.
Stefanovic, B., Pike, G.B., 2004. Diffusion and. Exch. Models 723, 716–723.
Stephan, K.E., Weiskopf, N., Drysdale, P.M., Robinson, P.A., Friston, K.J., 2007. Comparing hemodynamic models with DCM. NeuroImage 38, 387–401. ST - Comparing hemodynamic models with DC.
Stroman, P.W., Krause, V., Malisza, K.L., Frankenstein, U.N., Tomanek, B., 2001. Characterization of contrast changes in functional MRI of the human spinal cord at 1.5 T. Magn. Reson Imaging 19, 833–838.
Stroman, P.W., Krause, V., Malisza, K.L., Frankenstein, U.N., Tomanek, B., 2002. Extravascular proton-density changes as a non-BOLD component of contrast in fMRI of the human spinal cord, 127, 122–127.
Stroman, P.W., Tomanek, B., Krause, V., Frankenstein, U.N., Malisza, K.L., 2003. Functional magnetic resonance imaging of the human brain based on signal enhancement by extravascular protons (SEEP fMRI). Magnetic Reson. Med. 49, 433–439.
Triantafyllou, C., Wald, L.L., Hoge, R.D., 2011. Echo-time and field strength dependence of BOLD reactivity in veins and parenchyma using flow-normalized hypercapnic manipulation. PLoS ONE 6 e24519–e24519.
Uludag, K., Blinder, P., 2017. Linking Brain Vascular Physiology to Hemodynamic Response at Ultra-high Field MRI. Submitted.
Uludağ, K., Dubowitz, D.J., Yoder, E.J., Restom, K., Liu, T.T., Buxton, R.B., 2004. Coupling of cerebral blood flow and oxygen consumption during physiological activation and deactivation measured with fMRI. NeuroImage 23, 148–155.
Uludağ, K., Müller-Bierl, B., Uğurbil, K., 2009. An integrative model for neuronal activity-induced signal changes for gradient and spin echo functional imaging. NeuroImage 48, 150–165.
van Zijl, P.C.M., Hua, J., Lu, H., 2012. The BOLD post-stimulus undershoot, one of the most debated issues in fMRI. NeuroImage 62, 1092–1102.

Vidorreta, M., Wang, Z., Rodríguez, I., Pastor, M.A., Detre, J.A., Fernández-Seara, M.A., 2013. Comparison of 2D and 3D single-shot ASL perfusion fMRI sequences. NeuroImage 66, 662–671.
Yacoub, E., Duong, T.Q., Van De Moortele, P.-F., Lindquist, M., Adriany, G., Kim, S.-G., Uğurbil, K., Hu, X., 2003. Spin-echo fMRI in humans using high spatial resolutions and high magnetic fields. Magn 49, 655–664.
Yacoub, E., Le, T.H., Ugurbil, K., Xiaoping, H., 1999. Further evaluation of the initial negative response in functional magnetic resonance imaging. Magnetic Reson. Med. 41, 436–441.
Yacoub, E., Shmuel, A., Pfeuffer, J., Moortele, P.-F.V.D., adriany, G., 2001. Investigation of the initial dip in fMRI at 7 Tesla. NMR Biomed. 14, 408–412.
Yacoub, E., Ugurbil, K., Harel, N., 2006. The spatial dependence of the poststimulus undershoot as revealed by high-resolution BOLD- and CBV-weighted fMRI. J. Cereb. Blood Flow Metabol. Off. J. Int. Soc. Cereb. Blood Flow Metabol. 26, 634–644.
Zhao, F., Jin, T., Wang, P., Kim, S.-G., 2007a. Improved spatial localization of post-stimulus BOLD undershoot relative to positive BOLD. NeuroImage 34, 1084–1092.
Zhao, J.M., Clingman, C.S., Na, M.J., Kauppinen, R.A., Zijl, P.C.M.V., 2007b. Oxygenation and hematocrit dependence of transverse relaxation rates of blood at 3T, 596, 592–596.